Title
A Phase Field Model for Cell Shapes : : Gamma-Convergence and Numerical Simulations

Author
Banham, Timothy

Publication Date
2013

Peer reviewed|Thesis/dissertation

UNIVERSITY OF CALIFORNIA, SAN DIEGO

A Phase Field Model for Cell Shapes: Gamma-Convergence and Numerical Simulations

A dissertation submitted in partial satisfaction of the
requirements for the degree
Doctor of Philosophy

in

Mathematics

by

Timothy Banham

Committee in charge:

Professor Bo Li, Chair
Professor Li-Tien Cheng
Professor Eric Lauga
Professor Lei Ni
Professor Daniel Tartakovsky

2013

The dissertation of Timothy Banham is approved, and it is acceptable in quality and form for publication on microfilm and electronically:

_____

_____

_____

_____

_____

Chair

University of California, San Diego

2013

DEDICATION

To Him.

EPIGRAPH

Scientia inflat
charitas vero dificat.
—1 Cor 8:1

TABLE OF CONTENTS

Signature Page iii

Dedication iv

Epigraph v

Table of Contents vi

List of Figures viii

Acknowledgements x

Vita xi

Abstract of the Dissertation xii

Chapter 1 Introduction 1
- 1.1 Mathematical Modeling of Cell Membranes 1
  - 1.1.1 Shear and Stretch 2
  - 1.1.2 Bending 3
  - 1.1.3 Other Surface Energy Considerations 7
  - 1.1.4 Constraints 8
- 1.2 Phase Field Models 9
- 1.3 Gamma-Convergence 11
- 1.4 Main Results of this Dissertation 14

Chapter 2 The Two-Term Functional 17
- 2.1 Existence of Minimizers 17
- 2.2 Gamma-Convergence 19
  - 2.2.1 Definitions and Main Theorem 19
  - 2.2.2 Proof of Theorem 2.2: Part 1 20
  - 2.2.3 Proof of Theorem 2.2: Part 2 22
- 2.3 Convergence of Minimizers 26

Chapter 3 The Shao–Rappel–Levine Energy Functional: Including H^2 . . 29
- 3.1 Existence of Minimizers 30
- 3.2 Gamma-Convergence and Convergence of Minimizers 34
  - 3.2.1 Proof of Theorem 3.3: Part 1 35
  - 3.2.2 Proof of Theorem 3.3: Part 2 36
  - 3.2.3 Minimizers Converge to Minimizers 38

Chapter 4 Numerical Simulations 40
4.1 Finite Difference Method for 3D Radially Symmetric Cells 40
4.2 2D Simulations Using the Fourier Spectral Method . . . 43
4.2.1 Schemes 43
4.2.2 Results 45
4.3 3D Simulations: Shapes and Betti Numbers 49
4.3.1 Setup 49
4.3.2 Results 50
4.3.3 Classification of Configurations with Betti Numbers 56

Chapter 5 Conclusions and Future Directions 59
5.1 Summary 59
5.2 Future Problems 60

Bibliography 63

LIST OF FIGURES

Figure 1.1: A lipid bilayer. 1
Figure 1.2: Shear and stretch of lipid bilayer. 2
Figure 1.3: Bilayer undergoing bending. 3
Figure 1.4: Volume element from bent piece of area. 4
Figure 1.5: Lipid as a spring. 5
Figure 1.6: How bending affects the volume element. The ratio of volume elements is $(R+z)/R$. 6
Figure 1.7: Phase field compared to sharp interface. 9
Figure 1.8: A double well with minimums at 0 and 1. 9

Figure 2.1: Sketches of the functions $\psi_\epsilon(t)$ and $\phi_\epsilon(t)$. 23
Figure 2.2: 2D comparison of u_ϵ and the characteristic function limit. . . . 24

Figure 3.1: Sketch of Γ_ϵ. 37
Figure 3.2: Comparison of χ_A and u_ϵ. 37

Figure 4.1: The phase field as function of radius and time for $h = .1$ 41
Figure 4.2: The phase field as function of radius and time for $h = .8$. 42
Figure 4.3: Energy of u versus time for experiment with $h = .1$ initial profile . 42
Figure 4.4: Configurations started with a circle. 46
Figure 4.5: Configurations started with a "bean". 47
Figure 4.6: Configurations started with an ellipse. 48
Figure 4.7: Evolution of the 3D phase field. Initial profile is a sphere. . . . 50
Figure 4.8: Evolution of the 3D phase field. Initial profile is an ellipsoid. Grey lines show the boundary of the interior regions and the shape of the back side of the configuration. 51
Figure 4.9: Configurations started with an ellipsoid. 52
Figure 4.10: Configurations started with a sphere. 53
Figure 4.11: Configurations started with a blood cell, dented bubble, or a parachute shape. 54
Figure 4.12: Energy versus time plots for selected starting configurations and area-to-volume ratios. From top to bottom: parachute with A/V of 12, ellipsoid with A/V of 7, blood cell with A/V of 6, and sphere with A/V of 8. 55
Figure 4.13: Energy versus Area-to-Volume ratio plot for simulations that start with an ellipsoid. 56

Figure 4.14: Table 1 of Betti numbers for minimizers. VA = Volume-to-area ratio, P = Initial configuration was dented bubble (see first diagram in figure 4.11), S = Initial configuration was sphere, E2 (3) = Initial configuration was ellipsoid with length 2 (3) times it width, BC = Initial configuration was blood cell (see fourth diagram in figure 4.11). 57
Figure 4.15: Table 2 of Betti numbers for minimizers. 58

ACKNOWLEDGEMENTS

Thank you Bo for your guidance.

Thank you Michael, Jiayi, Shenggao, and Yanxiang for good conversations.

Thank you Stephen and Johannah for telling me to go for the gold.

Thank you Phillip, William, Hillary, Faith, Joseph, Thomas, Laura, Trish, Hope, Emma, Michael for your support.

Thank you friends at Laurel for your love and for showing me how to serve.

Thank you CG for your love and for teaching me commitment.

Thank you Chris, Gordon, and Peter for being true friends.

VITA

2007	B. S. in Mathematics, *College Honors*, University of Washington, Seattle
2007	B. S. in Physics, University of Washington, Seattle
2010	Masters of Arts in Mathematics, University of California, San Diego

ABSTRACT OF THE DISSERTATION

A Phase Field Model for Cell Shapes:
Gamma-Convergence and Numerical Simulations

by

Timothy Banham

Doctor of Philosophy in Mathematics

University of California, San Diego, 2013

Professor Bo Li, Chair

This dissertation studies two phase field energy functionals used in the modeling of vesicle shape: the Shao–Rappel–Levine (SRL) functional and the Seifert functional. In both functionals the vesicle is conceived as phase field or "diffuse interface" surface. The minimizing diffuse interface surfaces of the SRL functional have minimal bending and surface area and satisfy an enclosed volume constraint. On the other hand, minimizing diffuse interface surfaces of the Seifert functional have minimal bending and satisfy both a surface area constraint and an enclosed volume constraint. In the first three chapters, we prove Gamma-convergence of the SRL functional to a sharp interface functional and we prove that minimizers of the phase field functional converge to minimizers of this sharp interface functional.

Since the original functional used to find vesicle shape is a sharp interface functional, these analytical results are significant because they establish an equivalence between the phase field and the sharp interface formulations. In the fourth chapter, we run simulations using the Semi-Explicit Fourier Spectral Method to find minimizers of both phase field functionals. We discover and catalog a variety of 2D and 3D minimizing shapes, classify these minimizers with Betti numbers, and make some observations about how the phase field evolves to reach these minimizers. Our numerical work is significant for three reasons: we recover many of the vesicle shapes that have been observed experimentally; we discover several new stable shapes with interesting topology; and our program proves to be a useful tool for finding surfaces with minimal bending energy for given area and volume constraints. In the fifth and final chapter, we discuss future studies.

Chapter 1

Introduction

1.1 Mathematical Modeling of Cell Membranes

The cell membrane of most organisms is composed of lipids. A lipid is a molecule composed of two parts: a hydrophilic head and a tail composed of two hydrophobic chains; *cf.* Figure 1.1. Because of their tails' hydrophobia, lipids floating in a solution spontaneously group together to form a lipid bilayer: a double layered sheet composed of lipids with tails facing inward and heads facing the solution [18]. Because the edges of these sheets are hydrophobic, the lipid bilayer sheets form large "bag-like" surfaces without edges called vesicles.

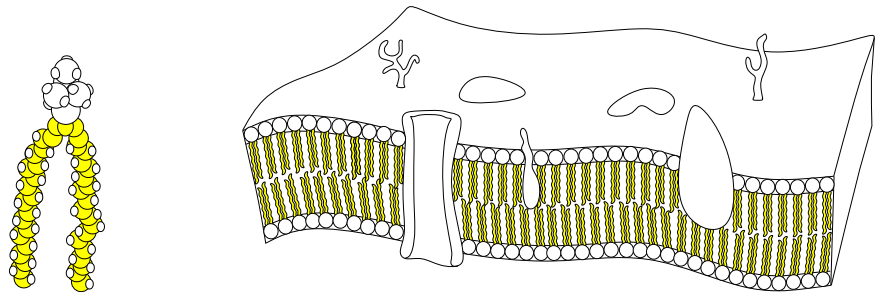

A: A lipid. B: Cell wall composed of lipids.

Figure 1.1: A lipid bilayer.

Vesicles typically take the form of spheres or ellipsoids suggesting that curvature and surface tension determine the bilayer's large scale shape. A curvature

model introduced by Canham: 1970 and Helfrich: 1973 and popularized by Seifert and Lipowsky has been the predominant model for vesicle shape since the 1970s [7, 17, 30, 35]. In this model, the vesicle shape is determined by finding the surface that minimizes a surface energy functional. The vesicle is represented by a closed surface Γ with total surface area A and enclosing a volume V. The configuration energy of this surface is

$$E[\Gamma] = \int_\Gamma (H - H_0)^2 dS \quad \text{subject to } V = V_0 \text{ and } A = A_0,$$

where H_0, V_0 and A_0 are constants. Let us look at how this model is derived from our understanding of the lipid bilayer.

1.1.1 Shear and Stretch

Lipid bilayers exist in two states: a gel state or a fluid state. Most biological membranes are in the fluid state. In this state, lipids can diffuse within the membrane very quickly (3×10^{-8} cm^2/sec) [22]. This fluidity indicates that shear strain costs negligable energy. In the study of lipid bilayers there is typically no consideration of shear stress; *cf.* Figure 1.2.

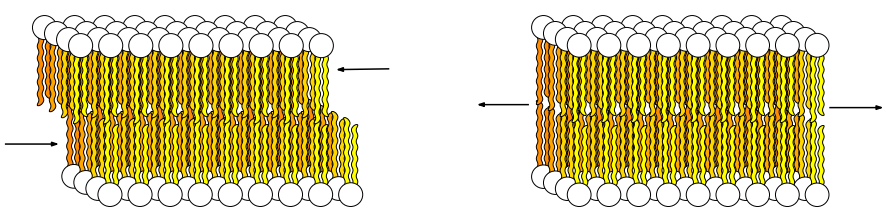

A: Bilayer undergoing shear. B: Bilayer undergoing stretch.

Figure 1.2: Shear and stretch of lipid bilayer.

Consider another type of deformation: stretching. For a two dimensional sheet of lipids, stretching strain comes from a change in the area of the sheet. Experiments [29] show that when a lipid bilayer is stretched, it does so elastically. Elasticity theory states that to the lowest order the energy change is given by the equation

$$E_{stretch} = \frac{1}{2} K_s \frac{(dA - dA_0)^2}{dA_0}.$$

Here K_s is the stretching modulus and $dA - dA_0$ is the deviation of the area element dA from some preferred area dA_0. Experiments testing this theory measure the preferred area of the head of a single lipid at 57 nm^2 [18] and the stretching modulus for a bilayer is $80 - 200$ mJ/m^2 [18].

Though we can measure the stretching modulus and accurately model the stretching as a square of the deviation, in practice, stretching is rarely considered when finding the large scale shape of a vesicle. There are three reasons for this. Firstly, compared to other thin sheets the lipid bilayer is very soft (on the same order of the surface tension of liquids), so while its shape can be deformed easily, the lipid bilayer will typically tear before it stretches very much from the preferred area. Secondly, because that lipid tails are hydrophobic, they do not leave the bilayer or hang out in the solution ready to be absorbed into the bilayer. Lastly, the energetic costs of stretching are much higher than that of bending.

Most models reasonably assume that the number of lipids in the bilayer is constant and consider the surface area fixed. We will continue the discussion of enforcing this constraint in the subsection on constraints. It should be noted that while vesicles maintain surface area, cells are more complex. For example, processes like endocytosis and exocytosis can result in a change of the cell's surface area.

1.1.2 Bending

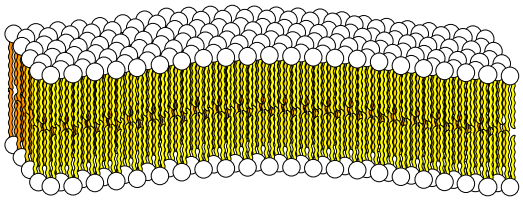

Figure 1.3: Bilayer undergoing bending.

If the bilayer is treated as a surface, bending is characterized by curvature. A connection between curvature and membrane shape was first outlined by physicists Canham [7] and Helfrich [17] in the early 1970s. Helfrich proposed the following Hamiltonian (energy functional) for the lipid bilayer considered as a

surface Γ:

$$E[\Gamma] = \int_\Gamma \left[\kappa_b (H - H_0)^2 + \kappa_g K\right] dS.$$

Here $H = (c_1 + c_2)/2$ is the mean curvature of the surface element with c_1 and c_2 the two principal curvatures, H_0 is a constant called the spontaneous curvature, and $K = c_1 c_2$ is the Gaussian curvature of the surface element. By the Gauss–Bonnet Theorem the total Gaussian curvature over a surface without boundary, $\int_\Gamma K dS$, is proportional to the Euler characteristic of the surface. Since in most cases the vesicle evolution does not involve change in genus, this total Gauss term is a constant and can be omitted.

Three distinct starting assumptions can independently produce this bending Hamiltonian. They are:

1. The heads want to maintain a preferred flat configuration and resist curvature of any sort [17];

2. The individual lipids act like springs [30] and the membrane's volume is constrained;

3. The bulk layer is composed of an elastic material [11].

Assumption 1 was behind Helfrich's orginal derivation of the Hamiltonian.

Bending from Lipids as Springs

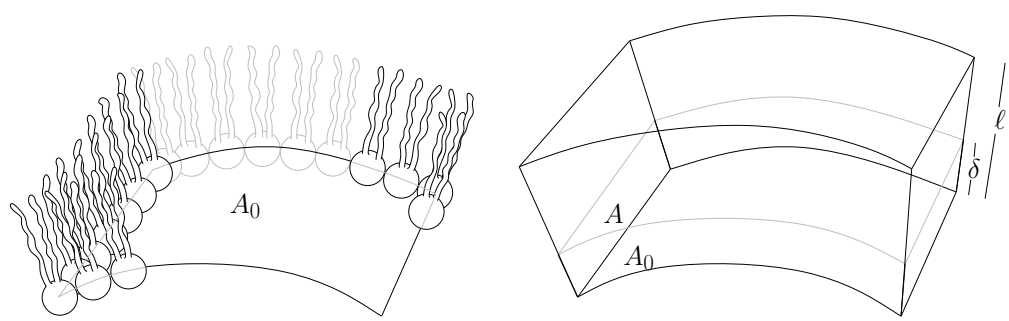

A: Define A_0 for a lipid layer. B: Estimate volume from area.

Figure 1.4: Volume element from bent piece of area.

Consider the lipids whose heads face the interior of the vesicle. Now consider the surface that corresponds to the region of space containing these heads; *cf.* Figure 1.4. Take a square piece of this surface with area A_0. The area, A, of the parallel surface distance δ from A_0 is, to the second order in δ [30],

$$A = A_0(1 + 2H\delta + K\delta^2).$$

If we add up these slices from $\delta = 0$ to $\delta = \ell$ where ℓ is the thickness of the bilayer, we get the volume of a piece of the bilayer:

$$V = A_0 \left(\ell + H\ell^2 + K\frac{\ell^3}{3} \right).$$

Since there is experimental evidence that lipid molecules maintain their volume [10] and as mentioned before the lipid molecules have a prefered head area [18], we assume V and A_0 stay fixed and that $\ell_0 \equiv V/A_0$ is a constant. Now we can solve this equation for ℓ. Up to the third order of ℓ_0 the solution is

$$\ell = \ell_0 + \ell_0^2 H + 2\ell_0^3 - \frac{1}{3}\ell_0^3 K.$$

In this model we assume the lipids act like springs; *cf.* Figure 1.5.

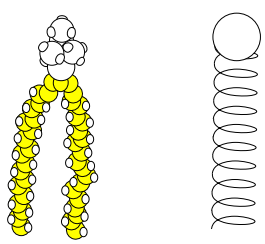

Figure 1.5: Lipid as a spring.

Therefore, we insert our ℓ as a function of curvature into a Hooke's law with ℓ_s as the lipid's preferred length and caclulate the bending energy e_{bend}. Expanding in the lowest orders of H and K, we get:

$$\begin{aligned} e_{bend} &= \frac{1}{2}k_s(\ell - \ell_s)^2 = \frac{k_s\ell_0^2}{2}\left((H - H_0)^2 - \frac{2H_0\ell_0}{3}K \right) \\ &= \kappa_b(H - H_0)^2 + \kappa_g K. \end{aligned}$$

where $H_0 \equiv (\ell_0 - \ell_s)/\ell_0^2$ is called the "spontaneous curvature". We'll discuss the meaning of this quantity in the next section. Summing this energy over the whole surface we recover the aforementioned curvature Hamilitonian:

$$E[\Gamma] = \int_\Gamma \left[\kappa_b (H - H_0)^2 + \kappa_g K\right] dS.$$

Bending from Volume Deformation

Let us derive the curvature Hamilitonian given the third assumption. To the lowest order the elastic energy depends on the change in the volume, $dV - dV_0$, quadratically:

$$E_{bend} = \frac{1}{2} Y \frac{(dV - dV_0)^2}{dV_0}.$$

Here Y is the elastic modulus. Assuming a sheet with width L, length L, and thickness h is curved in one direction with radius R, we can calculate the bending energy per area; *cf.* Figure 1.6.

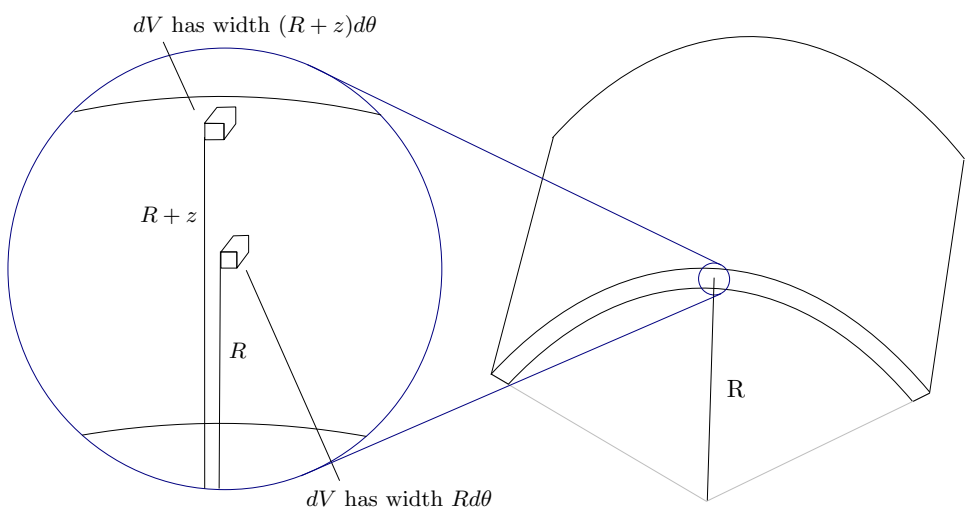

Figure 1.6: How bending affects the volume element. The ratio of volume elements is $(R+z)/R$.

$$e_{bend} = \frac{E_{bend}}{L^2} = \frac{1}{L^2} \int_0^L \int_0^L \int_{-h/2}^{h/2} \frac{1}{2} Y \frac{((1 + z/R)dxdydz - dxdydz)^2}{dxdydz}$$
$$= \frac{1}{2} Y \int_{-h/2}^{h/2} \left(\frac{z}{R}\right)^2 dz = \frac{Yh^3}{24R^2} \sim \frac{1}{R^2}.$$

Assuming Y and h are constants, we see that the energy per unit area depends on the curvature squared. Let's combine the Y and h into one coefficient, $\kappa_b = Yh^3/24$.

$$e_{bend} = \kappa_b \frac{1}{R^2} = \kappa_b c^2.$$

This sheet is only curved around one axis, so it only involves curvature in one direction $c = 1/R$. We need to generalize to the case where it is curved in more than one direction. For a two dimensional surface, the principal curvatures, c_1 and c_2 contain all the information about how such a surface could be curved. Assume the surface is isotropic and that the energy is a quadratic function of the curvatures. The quantities that enter into the energy then are c_1c_2 and $(c_2 + c_1)^2$. Thus, a natural generalization of equation (1.1.2) is:

$$e_{bend} = a \cdot (c_1 + c_2)^2 + b \cdot c_2c_1 = \kappa_b H^2 + \kappa_g K.$$

Taking this per surface area energy we can now write an expression for the total bending energy of a surface:

$$E[\Gamma] = \int_\Gamma \left(\kappa_b H^2 + \kappa_g K\right) dS.$$

1.1.3 Other Surface Energy Considerations

There are several other ways surface energy can be implimented into the energy Hamiltonian. Firstly, if we know the number of lipids in both layers, call them N^+ and N^-, then we can assume the expected area difference between the two layers to be proportional to their difference: $\Delta A_0 \propto N^+ - N^-$. Since curvature is related to area change: $\Delta A \approx hM$, where h is the thickness of the bilayer and M is its total mean curvature $\int_\Gamma HdS$, and this gives us an area difference elasticity:

$$E_{\text{area diff}} = \kappa_{ae} \left(\Delta A - \Delta A_0\right)^2 \approx (M - M_0)^2.$$

Secondly, each layer in the lipid bilayer may be composed of different types of lipids each with a preferred area. Such a bilayer would have a natural preferred curvature. This gives a nice interpretation of the aforementioned "spontaneous" curvature H_0 and the corresponding bending energy:

$$E_{stretch} = \int_\Gamma \kappa_b \left(H - H_0\right)^2 dS.$$

So far we have focused on how energy concerns give us the stationary states of vesicle composed of lipid bilayers. The study of how cells move, particularly along a substrate, is an active area of research. Cell dynamics are implemented in Shao, Rappel, and Levine's PRL paper [33] by coupling the phase field functional with two diffusion equations involving concentrations of actin bundles and actin filments. This is consistent with the cytoskeletal model, one of two popular models for cell movement. There is much we have to learn about actin's role in cell movement, but the Shao–Rappel–Levine model gives us one way of implementing it into a model of cell movement.

1.1.4 Constraints

Area

In the discussion of stretching, we argued that, since the lipid bilayer is fragile under stretching and contains a fixed number of lipids, the surface area should be considered fixed. Constant surface area is typically enforced by either a Lagrange multiplier or an energy penalty term of the form:

$$E_{stretch} = \kappa_s \left(\int_\Gamma dS - A_0 \right)^2 .$$

Volume

Recent experimental evidence [21] indicates that over short time scales cells maintain volume (or in a 2D context: area). In the past, this constant volume was enforced by a Lagrange multiplier. In the Shao–Rappel–Levine model the volume constraint is enforced by an energy penalty term of the form $(V - V_0)^2$. As we will see, this penalty formulation produces better numerical results than the Lagrange multiplier formulation.

1.2 Phase Field Models

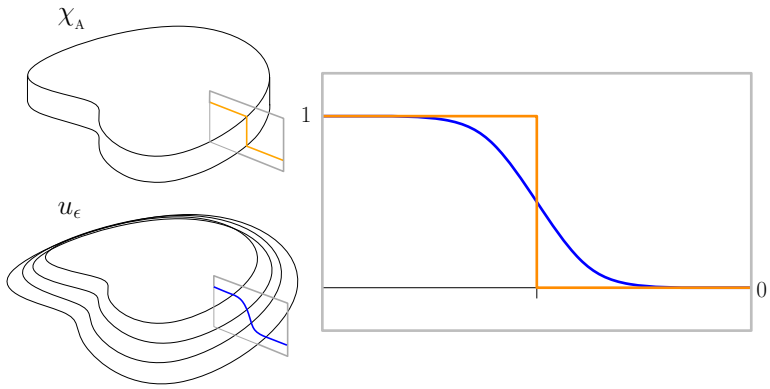

Figure 1.7: Phase field compared to sharp interface.

Phase field models were first introduced by van der Waals [36] in his 1893 work on liquid-vapour interfaces. The idea is simple: represent a sharp interface between two substances with a smooth "phase" function, $\phi(x)$, that is 1 for one of the substances and, 0 for the other, and quickly transitions from 1 to 0 at the interface; *cf.* Figure 1.7. We find the phase field function and configuration of the two substances it represents by minimizing an energy functional. Ideally, minimizers of this energy functional are the physically realistic equilibrium configurations of the two substances. The canonical example here is the Cahn–Hilliard functional [6].

$$SA_\epsilon[u] = \int_\Omega \left[\frac{\epsilon}{2}|\nabla u|^2 + \frac{1}{\epsilon}W(u)\right] dx, \tag{1.1}$$

where $W(t) = t^2(1-t)^2$ is a double well potential.

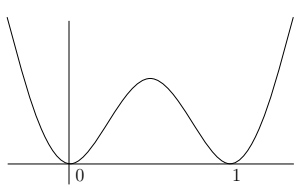

Figure 1.8: A double well with minimums at 0 and 1.

The points in Ω for which u takes a value other than 1 and 0 or u is not smooth contribute to the energy via the double well or gradient squared term.

Thus, if u is to minimize this functional it must be mostly 0 or 1 over the domain and have few jumps and discontinuities. These two effects combine into one: for small ϵ, minimizers of this functional turn out to have small "transition" region $\{x \in \Omega \mid u(x) \neq 1, 0\}$. By taking a 1/2 level set of u, one can think of this transition region as a surface. In fact, as it will be shown later, as ϵ gets smaller, these level sets converge to a surface of minimal area.

Phase field functions are used in the place of sharp interface formulations for several reasons. The most prominant reason is to bypass the difficulties sharp interface models encounter with surface intersection and topological change. Because of its versitility in this regard, the phase field method has been applied to a wide variety of physical problems: fluid dynamics [1], solidification [25], fracture [19], imaging analysis, grain growth [37], and cell shape, to name a few.

For fluid problems the Cahn–Hilliard functional is coupled with the Navier–Stokes equation. The use of the Cahn–Hilliard functional in the fluid context makes sense: anyone who has mixed oil with water knows that fluid to fluid interfaces try to minimize their surface area. In some phase field simulations without surface area constraint or surface area minimization, sometimes the Cahn–Hilliard term is still employed to smooth out the small scale wrinkles or enforcing the minimizer to be mostly the minimizing values of the double well potential.

In the context of cell modeling, the following phase field functional is often used [33, 34, 23]:

$$B_\epsilon[u] = \int_\Omega \frac{1}{\epsilon}\left[-\epsilon\Delta u + \frac{W'(u)}{\epsilon}\right]^2 dx.$$

This functional is called the bending energy functional, named so because for small ϵ the level sets of the minimizers, considered as surfaces, are minimizers of the Willmore Energy, $\int_\Gamma H^2 dS$, on surfaces. This makes intuitive sense if we take the variational derivatives of the diffuse and sharp interface functional: Let Γ_t^ϕ be the surface Γ allowed to flow for some small time t in the normal direction n with magnitude ϕ:

$$\Gamma_t^\phi = x + t\phi(x)n \qquad (x \in \Gamma).$$

Using Γ_t^ϕ we compute the variational derivative of surface area:

$$\frac{d}{dt}\left(\int_{\Gamma_t^\phi} dS\right)\Bigg|_{t=0} = \int_\Gamma H\phi dS.$$

Compare this with the variational derivative of SA_ϵ:

$$\frac{d}{dt}SA_\epsilon[u+ht]|_{t=0} = \int_\Omega \left[-\epsilon\Delta u + \frac{W'(u)}{\epsilon}\right] h\, dx.$$

It seems reasonable to draw loose connection between

$$H \text{ and } \left[-\epsilon\Delta u + \frac{W'(u)}{\epsilon}\right]$$

and hypothesize that minimizers of $\int_\Gamma H^2 dS$ correspond to minimizers of

$$\int \left[-\epsilon\Delta u + \frac{W'(u)}{\epsilon}\right]^2 dx.$$

We will formalize the connection between the sharp interface Willmore energy and the phase field functional B_ϵ in the next section.

1.3 Gamma-Convergence

The idea of Gamma-convergence was put forth by the eminent Italian mathematician De Giorgi in 1973 [4, 9].

Definition 1.3.1 (Gamma-Convergence)**.** *Let X be a Banach space and $\{E_\epsilon\}_{\epsilon>0}$ and E_0 functionals from X to $\bar{\mathbb{R}} = \mathbb{R}\cup\{-\infty,\infty\}$ where $\{\epsilon\}$ is a sequence $\{\epsilon_n\}_{n=1}^\infty$ with $\epsilon_n \downarrow 0$. E_ϵ Gamma-coverges to E_0 as $\epsilon \to 0$ if the following two conditions hold:*

1. *Liminf inequality:* $\liminf_{\epsilon\to 0} E_\epsilon[u_\epsilon] \geq E_0[u_0] \quad \forall\, u_\epsilon \to u_0$ *in* X.
2. *Limsup inequality:* $\forall u_0 \in X$, $\exists\, u_\epsilon \to u_0$ *in* X *such that* $\limsup_{\epsilon\to 0} E_\epsilon[u_\epsilon] \leq E_0[u_0]$.

In this case, we call E_0 the Gamma-limit of E_ϵ.

Gamma-convergence is an appealing concept because it is a sufficient condition for the convergence of minimizers of the sequence of functionals E_ϵ to minimizers of E_0 via the following argument.

1. Take the sequence of minimizers for $E_\epsilon[\cdot]$ and label them u_ϵ.
2. Assume $u_\epsilon \to u \in X$.
3. For any other $v \in X$ there exists a sequence $v_\epsilon \to v$ such that the following inequality holds.

$$E[v] \geq \limsup_{\epsilon \to 0} E_\epsilon[v_\epsilon] \geq \limsup_{\epsilon \to 0} E_\epsilon[u_\epsilon] \geq \liminf_{\epsilon \to 0} E_\epsilon[u_\epsilon] \geq E[u]$$

4. $\inf_{v \in X} E[y] \geq E[u]$ since $E[v] \geq E[u]$ for all $v \in X$.
5. Since $u \in X$, $\min_{v \in X} E[v] = E[u]$.

Gamma-convergence turns the problem of showing there exists a minimizer of E_0 into the problem of showing minimizers of E_ϵ exist for all ϵ. In turn, proving existence of minimizers of E_ϵ is done by showing coercivity or equi-mild coercivity [4] of E_ϵ for each ϵ.

Definition 1.3.2. *Let X be a Banach space. A sequence $\{E_\epsilon\}_{\epsilon>0}$ of functional on X is equi-mildly coercive if there exists a non-empty compact set $K \subset X$ such that $\inf_K E_\epsilon = \inf_X E_\epsilon$ for all $\epsilon > 0$.*

Though Gamma-convergence is a very powerful tool, it is not common to prove Gamma-convergence for functionals in full generality. In particular, it turns out to be quite difficult to construct a convergent sequence of functions, u_ϵ, which satisfies the limsup property for limit function u that is not very smooth. One can however prove this inequality for u with properties that are nice, like u is the indicator function on a set with Lipshitz or C^2 boundary. If, in addition, one can prove the mimimum of the limit energy, $E_0[\cdot]$ over u with nice properties is the same as the minimum of $E_0[\cdot]$ over all functions, one can prove that minimizers converge to minimizers.

Because it establishes a clean connection between different minimization problems, Gamma-convergence is used in the Calculus of Variations and modeling contexts to establish a relationship between phase field problems and sharp interface problems. After inventing the concept of Gamma-convergence, De Giorgi made several conjectures on the Gamma-convergence of different types of functionals. Those [2, 28] working with the phase field method modified one such conjecture for the purpose of working with phase field problems.

Modified De Giorgi Conjecture Consider a set $\Omega \subseteq \mathbb{R}^n$, let $W(t) := (1-t^2)^2$ and define for $\delta > 0$ functionals $\mathcal{F}_\delta : L^1(\Omega) \to \mathbb{R}$ by

$$\mathcal{F}_\delta[u] := \int_\Omega \left[\frac{\delta}{2}|\nabla u|^2 + \frac{1}{\delta}W(u)\right] dx + \int_\Omega \frac{1}{\delta}\left[-\delta\Delta u + \frac{W'(u)}{\delta}\right]^2 dx, \tag{1.2}$$

if $u \in W^{2,2}(\Omega)$, and $\mathcal{F}_\delta[u] := \infty$ if $u \in L^1(\Omega)\backslash W^{2,2}(\Omega)$. Then, given $\sigma := \int_{-1}^1 \sqrt{2W}$, for any $\chi = 2\chi_E - 1$ with measurable $E \subseteq \Omega$, $\partial E \cap \Omega \in C^2$, the Gamma-limit as $\delta \to 0$ of $\mathcal{F}_\delta[u]$ is

$$\sigma\mathcal{H}_{n-1}(\partial E \cap \Omega) + \sigma \int_{\partial E \cap \Omega} |\mathbf{H}_{\partial E}|^2 d\mathcal{H}_{n-1}. \tag{1.3}$$

Here $\mathcal{H}_{n-1}$ is the (n-1)-dimensional Hausdorff measure and $\mathbf{H}_{\partial E}$ is the mean curvature vector of ∂E. The first term in this functional $\mathcal{F}_\delta$ is the familiar Cahn–Hilliard functional and second term is typically called the bending energy. We would expect from the gradient and $W(u)$ terms that as ϵ goes to 0, the phase field function u becomes sharper and its level sets converge to a surface of minimal area. In his influential 1985 paper [26] Modica showed just that: the Gamma-limit of Cahn–Hilliard phase field functional is:

$$E_0[\chi_A] = \int_\Omega |D\chi_A| dx \equiv \sup_g \left\{ \int_\Omega \chi_A(x) \sum_i \frac{\partial g}{\partial x_i}(x) dx \ : g \in C_0^\infty(\Omega, \mathbb{R}^n), |g| \leq 1 \right\}. \tag{1.4}$$

A couple comments:

- $\int |Du| dx$ restricted to characteristic sets is denoted by P_Ω, and is called the perimeter measure on sets. This notation was introduced in 1960 by Fleming and Rishel [16] and used by Modica. $P_\Omega(B) \leq \mathcal{H}_{n-1}(\partial B)$ with equality if B has Lipschitz boundary.

- $\int |Du|dx$ is the BV norm. Consider it a weak gradient, for when $u \in W^{1,1}(\Omega)$, $\int |Du|dx = \int |\nabla u|dx$.

The convergence of the bending energy is more tricky. Heuristically it makes sense, as we outlined in the previous section, but the formal proof took many years to develop. In 1993, Bellettini [3] proved the limsup inequality for the bending energy given a nice limit funcation. The liminf inequality and resulting conjecture were proved by Roger and Schätzle [28] in 2006.

Inspired by the Shao–Rappel–Levine cell model, we have been looking at the Gamma-convergence of energy functional $\mathcal{F}_\delta$ adding a volume constraint term:

$$\begin{aligned}\mathcal{E}_\epsilon[u] &= \mathcal{E}_{surfacearea}[u] + \mathcal{E}_{volume}[u] + \mathcal{E}_{bending}[u] \\ &= \gamma_s \int_\Omega \left[\frac{\epsilon}{2}|\nabla u|^2 + \frac{1}{\epsilon}W(u)\right] dx + M(\epsilon)\left(\int_\Omega u\,dx - V\right)^2 \\ &\qquad + \gamma_b \int_\Omega \frac{1}{\epsilon}\left[-\epsilon\Delta u + \frac{W'(u)}{\epsilon}\right]^2 dx.\end{aligned} \tag{1.5}$$

Here $W(t)$ is a standard double well potential, $M(\epsilon)$ is a function of $O(\frac{1}{\epsilon})$ or greater ($\frac{1}{\epsilon}$ or $\frac{1}{\epsilon^2}$), $\Omega \subset \mathbb{R}^n$ (n=2 or 3) is a bounded domain, and V is the ideal volume constant. For simplicity we take $\gamma_s = \gamma_b = 1$. This energy functional framework is also articulated in Shao's dissertation [34].

Since Gamma-convergence demonstrates equivalence of functionals, in the sense that the minimizers of $\mathcal{E}_\epsilon$, if they exist, are "close" (converging) to the minimizers of the limit $\mathcal{E}_0$, to establish the "equivalence" of the diffuse and sharp interface problems, as $\epsilon \to 0$, we would like to see the Shao–Rappel–Levine energy functional, $\mathcal{E}_\epsilon$, Gamma-converge to a sharp interface functional like

$$\mathcal{E}_0[\chi_A] = \begin{cases} \int |D\chi_A|dx + \int_{\partial A} |\mathbf{H}_{\partial A}|^2 d\mathcal{H}_{n-1} & \text{if } \int \chi_A dx = V, \\ \infty & \text{if } \int \chi_A dx \neq V. \end{cases} \tag{1.6}$$

1.4 Main Results of this Dissertation

A phase field model for cell shape was proposed by Shao, Rappel, and Levine in their 2010 PRL paper [33]. According to this model, for short term

time scales, a cell's membrane shape is determined by the cell's desire to minimize surface tension, minimize bending energy, maintain a constant volume, and decrease or increase according to the local concentration of actin filaments or actin bundles. These four properties of cell membranes are reflected in a rescaled partial differential equation (PDE) with four force terms.

$$\begin{aligned}\frac{\partial u}{\partial t} &= \left(-\Delta u + \frac{W'}{\epsilon^2}\right) - \left(-\Delta + \frac{W''}{\epsilon^2}\right)\left(-\Delta u + \frac{W'}{\epsilon^2}\right) \\ &\quad - M(\epsilon)\left(\int_\Omega u\,dx - V\right)|\nabla u| + (\alpha V - \beta W)|\nabla u|. \end{aligned} \tag{1.7}$$

Here V represents the ideal volume and $W(t) = (t-1)^2 t^2$ is a double well potential with minimums at 1 and 0. This encourages the phase field function, u, to take on 1 in the interior of the cell and 0 outside the cell. The first three terms (the surface area, bending energy, and volume constraint terms) come from the first variation of the aforementioned three term phase field energy functional. Current research on actin's role in cell movement [5] motivates the fourth term. This fourth term couples the phase field with the dynamic concentrations of actin filaments and actin bundles in the cell.

In this dissertation, we will analyze the the sharp interface limit of the functional and summarize the results of some numerical experiments performed with this phase field model.

In Chapter 2, we look at the 2-term functional, the phase field Shao–Rappel–Levine functional without the H^2 term or the actin term. In the first part, we prove existence of minimizers using standard theory from functional analysis (see Theorem 2.1.1). In the next part we prove Gamma-convergence of the 2-termed functional (see Theorem 2.2.1). This involves proving both the limsup and liminf estimates. Both proofs are modeled after the corresponding liminf and limsup estimate proofs in Modica [26] with some subtle but important changes to incorperate the volume constraint. In the last part we work out in detail a common feature of Gamma-convergence: that minimizers converge to minimizers.

In Chapter 3, we study the Shao–Rappel–Levine functional. In the first part of this section, we again prove existence of minimizers, building on our work in part 2, though this time our work is in the space H_0^2. In the next part we prove

Gamma-convergence of this 3-term functional for smooth functions. This involves proving both the limsup and liminf estimates. This time the proofs are modeled after the corresponding liminf and limsup estimate proofs in Roger and Schätzle [28] and Bellettini [2] respectively. In the last part of this section we work out future directions for how one might prove Gamma-convergence in full generality.

In Chapter 4, we run some numerical tests to find minimizers of two phase field functionals: the Shao–Rappel–Levine functional and a modified version we call the Seifert functional. In the first simulation, we find minimizers of the Shao–Rappel–Levine functional over a rotationally symmetric phase field in a 2D square domain. Starting with rings and circles, we see that the steady state solution is a sphere with volume equal to the constraint volume. We then use Semi-Implicit Fourier Spectral Method in 2D and 3D to find minimizers of both the the Shao–Rappel–Levine functional and the Seifert functional. We find a diverse array of minimizing configurations in both the 2D and 3D cases and classify these minimizers with Betti numbers.

In Chapter 5, we summarize our results and propose several interesting research directions and problems.

Chapter 2

The Two-Term Functional

The following will be assumed throughout this paper.

1. $0 < \epsilon < \epsilon_0$ where $\epsilon_0 \in (0,1)$ is fixed.
2. $W(t) := (t-1)^2 t^2$.
3. $c_0 = \int_0^1 \sqrt{W(t)}dt = 1/6$.
4. $\Omega \subset \mathbb{R}^3$ is bounded, open, and connected with $\partial\Omega \in C^1$.
5. $M(\epsilon)$ is a function of ϵ such that $M(\epsilon) = O(1/\epsilon)$ as $\epsilon \to 0$.

2.1 Existence of Minimizers

Theorem 2.1.1. *Let $V > 0$ be a constant, and fix $\epsilon > 0$. Define $E_\epsilon : L^1(\Omega) \to \mathbb{R}^+ \cup \{\infty\}$ by*

$$E_\epsilon[u] = \begin{cases} \displaystyle\int_\Omega \left[\frac{\epsilon}{2}|\nabla u|^2 + \frac{1}{\epsilon}W(u)\right] dx + M(\epsilon)\left(\int_\Omega u\,dx - V\right)^2 & \text{if } u \in H_0^1(\Omega), \\ \infty & \text{otherwise.} \end{cases} \tag{2.1}$$

There exists $u \in H_0^1(\Omega)$ such that

$$0 \le E_\epsilon[u] = \min_{v \in L^1(\Omega)} E_\epsilon[v] < \infty.$$

Proof of Theorem 2.1.1. Let

$$\alpha = \inf_{v \in L^1(\Omega)} E_\epsilon[v].$$

Since $E_\epsilon[v] \geq 0$ for all $v \in L^1(\Omega)$, $\alpha \geq 0$. If $v(x) \equiv 0$ $\forall x \in \Omega$, then $E_\epsilon[v] = M(\epsilon)V^2 > 0$. Thus, $\alpha \leq E_\epsilon[v] < \infty$. Let $u_k \in L^1(\Omega)$ $(k = 1,2,...)$ be such that

$$\lim_{k\to\infty} E_\epsilon[u_k] = \alpha.$$

Since

$$\int_\Omega \frac{\epsilon}{2}|\nabla u_k|^2\, dx \leq E_\epsilon[u_k] \to \alpha \quad \text{as} \quad k \to \infty.$$

we see that $\left\{\int_\Omega \frac{\epsilon}{2}|\nabla u_k|^2 dx\right\}_{k=1}^\infty$ is bounded. Moreover, $E_\epsilon[u_k] \to \alpha$ implies that $E_\epsilon[u_k]$ is finite for $k \geq k_0$ for some k_0. Therefore, we may assume that, without loss of generality, all $E_\epsilon[u_k]$ $(k = 1,2,...)$ are finite. Hence $u_k \in H_0^1(\Omega)$ by the definition of $E_\epsilon[\cdot]$. By Poincure's inequality, $\{||u_k||_{H_0^1(\Omega)}\}_{k=1}^\infty$ is bounded. Now $\{u_k\}$ has a subsequence not relabeled such that

$$u_k \rightharpoonup u \text{ in } H_0^1(\Omega),$$

$$u_k \to u \text{ a.e. } \Omega,$$

$$u_k \to u \text{ in } L^2(\Omega) \quad \text{for some } u \in H_0^1(\Omega).$$

Clearly,

$$M(\epsilon)\left(\int_\Omega u_k\, dx - V\right)^2 \to M(\epsilon)\left(\int_\Omega u\, dx - V\right)^2 \quad \text{as} \quad k \to \infty.$$

Fatou's Lemma implies that

$$\int_\Omega W(u)\, dx = \int_\Omega \lim_{k\to\infty} W(u_k)\, dx \leq \liminf_{k\to\infty} \int_\Omega W(u_k)\, dx.$$

Finally, since

$$\int_\Omega |\nabla u_k - \nabla u|^2\, dx = \int_\Omega |\nabla u_k|^2\, dx + \int_\Omega |\nabla u|^2\, dx - 2\int_\Omega \nabla u_k \cdot \nabla u\, dx \geq 0,$$

we have

$$\int_\Omega |\nabla u_k|^2\, dx \geq 2\int_\Omega \nabla u_k \cdot \nabla u\, dx - \int_\Omega |\nabla u|^2\, dx.$$

Thus

$$\begin{aligned}\liminf_{k\to\infty}\int_\Omega |\nabla u_k|^2\,dx &\geq \liminf_{k\to\infty} 2\int_\Omega \nabla u_k\cdot\nabla u dx - \int_\Omega |\nabla u|^2\,dx\\ &= 2\int_\Omega |\nabla u|^2\,dx - \int_\Omega |\nabla u|^2\,dx\\ &= \int_\Omega |\nabla u|^2\,dx.\end{aligned}$$

Combining all these, we obtain

$$\alpha = \liminf_{k\to\infty} E_\epsilon[u_k] \geq E_\epsilon[u] \geq \alpha.$$

Therefore, $E_\epsilon[u] = \alpha$. □

2.2 Gamma-Convergence

In this section we prove Gamma-convergence of the two term functional:

2.2.1 Definitions and Main Theorem

Definition 2.1. Characteristic function: χ_B is the characteristic function of $B \subset \mathbb{R}^n$. In other words, $\chi_B(x) = 1$ if $x \in B$ and $\chi_B(x) = 0$ otherwise.

Definition 2.2. The set of Lebesque measurable sets. Let S be the collection of characteristic functions χ_B of sets $B \subset \Omega$ that are Lebesgue measurable.

Definition 2.3. The energy functionals $E_0 : S \to \mathbb{R}^+ \cup \infty$ and $E_\epsilon : L^1(\Omega) \to \mathbb{R}^+ \cup \{\infty\}$.

$$E_0[\chi_B] = \begin{cases}\sqrt{2}c_0 P_\Omega(B) & \text{if } \int \chi_B dx = V,\\ \infty & \text{otherwise.}\end{cases}$$

$$E_\epsilon[u] = \begin{cases}\displaystyle\int_\Omega \left[\frac{\epsilon}{2}|\nabla u|^2 + \frac{1}{\epsilon}W(u)\right] dx + M(\epsilon)\left(\int_\Omega u\,dx - V\right)^2 & \text{if } u \in H_0^1(\Omega)\\ \infty & \text{otherwise.}\end{cases}$$

Theorem 2.2.1. *Define $E_0 : S \to \mathbb{R}^+$ and $E_\epsilon : L^1(\Omega) \to \mathbb{R}^+$ as in Definition 2.3.*

1. *Let $\{u_\epsilon\}$ be a sequence of functions in $H_0^1(\Omega)$ such that $u_\epsilon \to \chi_B$ in $L^1(\Omega)$. Then*

$$\liminf_{\epsilon\to 0} E_\epsilon[u_\epsilon] \geq E_0[\chi_B].$$

2. *Let $A \subset \Omega$ be open and non-empty, with ∂A Lipschitz continuous and $|dist(A, \partial\Omega)| > 0$. There exists a sequence $u_\epsilon \to \chi_A$ in L^1 such that*

$$\limsup_{\epsilon\to 0} E_\epsilon[u_\epsilon] \leq E_0[\chi_A]. \tag{2.2}$$

Proof of Theorem 2.2.1 uses the following lemmas and follows closely Propositions 1 and 2 in Modica [26].

Lemma 2.2.1 (Coarea formula: 3.4.3 Thm 2 from [15])**.** *Let $u : \mathbb{R}^n \to \mathbb{R}$ be Lipschitz and $f : \mathbb{R} \to \mathbb{R}$ Lebesgue measurable. Then for each Lebesgue measurable set $\Omega \subseteq \mathbb{R}^n$,*

$$\int_\Omega f(u(x))|Du(x)|dx = \int_{\mathbb{R}} f(t)\mathcal{H}_{n-1}\left(\{x \in \Omega : u(x) = t\}\right) dt.$$

Lemma 2.2.2 (Fleming–Rishel Formula: Theorem 1 from [16])**.** *Let $u : \mathbb{R}^n \to \mathbb{R}$ be locally Lebesgue measurable on $\Omega \subseteq \mathbb{R}^n$. Let $U_t = \{x \in \mathbb{R}^n : u(x) > t\}$ Then*

$$\int_\Omega |Du(x)|dx = \int_{\mathbb{R}} P_\Omega\left(U_t\right) dt = \int_{\mathbb{R}}\int_\Omega |D\chi_{U_t}|dxdt.$$

2.2.2 Proof of Theorem 2.2: Part 1

Proof. Assume $u \in H_0^1(\Omega)$ and define

$$Q_\epsilon[u] = \int_\Omega \left[\frac{\epsilon}{2}|\nabla u|^2 + \frac{1}{\epsilon}W(u)\right] dx.$$

Consider the truncated functions

$$\tilde{u}_\epsilon = \max\{0, min\{u_\epsilon, 1\}\}.$$

Clearly $Q_\epsilon[u_\epsilon] \geq Q_\epsilon[\tilde{u}_\epsilon]$ for each ϵ. If we prove

$$\liminf_{\epsilon\to 0} Q_\epsilon[\tilde{u}_\epsilon] \geq E_0[\chi_B],$$

then Part 1 follows by the following inequalities:

$$\liminf_{\epsilon\to 0} E_\epsilon[u_\epsilon] \geq \liminf_{\epsilon\to 0} Q_\epsilon[u_\epsilon] \geq \liminf_{\epsilon\to 0} Q_\epsilon[\tilde{u}_\epsilon] \geq E_0[\chi_B].$$

Define:

$$\begin{aligned}
\phi(t) &= \int_0^t W^{1/2}(s)ds, \\
w_\epsilon(x) = \phi(u_\epsilon(x)) &= \int_0^{u_\epsilon(x)} W^{1/2}(s)ds, \\
w_0(x) = \phi(\chi_B(x)) &= \int_0^{\chi_B(x)} W^{1/2}(s)ds.
\end{aligned}$$

By the following argument $w_\epsilon \to w_0$ in $L^1(\Omega)$.

$$\begin{aligned}
\|w_\epsilon - w_0\|_{L^1} &= \left| \int_\Omega \left(\int_0^{u_\epsilon(x)} W^{1/2}(s)\, ds - \int_0^{\chi_B(x)} W^{1/2}(s)\, ds \right) dx \right| \\
&= \int_\Omega \left| \int_{\chi_B(x)}^{u_\epsilon} W^{1/2}(s)\, ds \right| dx \\
&\leq \max_{0\leq s\leq 1} |W^{1/2}(s)| \int_\Omega |u_\epsilon - \chi_B|\, dx \to 0.
\end{aligned}$$

By Lemma 2.2.2,

$$\int_\Omega |Dw_0|dx = \int_{\mathbb{R}} P_\Omega\left(\{x \in \mathbb{R}^n : w_0(x) > t\}\right) dt = \phi(1)P_\Omega(B) = c_0 P_\Omega(B) \tag{2.3}$$

Convergence in $L^1(\Omega)$ is sufficient to establish the following inequality (see Lower-Semi-continuity of Variation Measure, p. 172 in Evans [15]):

$$\int_\Omega |Dw_0|dx \leq \liminf_{\epsilon\to 0} \int_\Omega |Dw_\epsilon|dx.$$

Thus:

$$\begin{aligned}
\int_\Omega |Dw_0|dx &\leq \liminf_{\epsilon\to 0} \int_\Omega |Dw_\epsilon|dx \\
&= \liminf_{\epsilon\to 0} \int_\Omega |W^{1/2}(u_\epsilon)||Du_\epsilon|dx \\
&\leq \liminf_{\epsilon\to 0} \frac{1}{2} \int_\Omega \left[\frac{\epsilon}{\sqrt{2}} |\nabla u_\epsilon|^2 + \frac{\sqrt{2}}{\epsilon} W(u_\epsilon) \right] dx \\
&\leq \liminf_{\epsilon\to 0} \frac{1}{\sqrt{2}} \int_\Omega \left[\frac{\epsilon}{2} |\nabla u_\epsilon|^2 + \frac{1}{\epsilon} W(u_\epsilon) \right] dx \\
&= \liminf_{\epsilon\to 0} \frac{1}{\sqrt{2}} Q_\epsilon[u_\epsilon].
\end{aligned} \tag{2.4}$$

Assume $\|\chi_B\|_{L^1} = V$. Then it follows from 2.3 and 2.4 that

$$\frac{1}{\sqrt{2}} E_0[\chi_B] = c_0 P_\Omega(B) \leq \liminf_{\epsilon \to 0} \frac{1}{\sqrt{2}} E_\epsilon[u_\epsilon].$$

Assume $\|\chi_B\|_{L^1} \neq V$. This makes

$$\liminf_{\epsilon \to 0} M(\epsilon) \left(\int_\Omega u_\epsilon \, dx - V \right)^2 = \infty.$$

Thus,

$$\begin{aligned}
\liminf_{\epsilon \to 0} E_\epsilon[u_\epsilon] &= \liminf_{\epsilon \to 0} \left(\int_\Omega \left[\frac{\epsilon}{2} |\nabla u_\epsilon|^2 + \frac{1}{\epsilon} W(u_\epsilon) \right] dx + M(\epsilon) \left(\int_\Omega u_\epsilon \, dx - V \right)^2 \right) \\
&\geq \liminf_{\epsilon \to 0} \int_\Omega \left[\frac{\epsilon}{2} |\nabla u_\epsilon|^2 + \frac{1}{\epsilon} W(u_\epsilon) \right] dx + \infty \\
&= \infty.
\end{aligned}$$

Since by definition $E_0[\chi_B] = \infty$ also, the inequality holds. □

2.2.3 Proof of Theorem 2.2: Part 2

Proof. We need to construct *one* sequence where inequality 2.2 holds. Construction of this sequence follows closely Modica's construction [26].

Let us define the signed distance function $d(x)$ and the function $\chi(t)$ as follows:

Definition 2.4. The signed distance function and step function:

$$d(x) = \begin{cases} -\text{dist}(x, \partial A) & \text{if } x \in A, \\ \text{dist}(x, \partial A) & \text{if } x \notin A. \end{cases} \tag{2.5}$$

$$\chi_0(t) = \begin{cases} 1 & \text{if } t < 0, \\ 0 & \text{if } t \geq 0. \end{cases}$$

It is easy to verify that $\chi_0(d(x)) = \chi_A(x)$ for any $x \in \Omega \backslash A$. Clearly

$$\int_\Omega [\chi_A(x) - \chi_0(d(x))] \, dx = 0.$$

Now we construct u_ϵ.

$$\psi_\epsilon(t) = \int_0^{1-t} \frac{\epsilon}{(2W(s) + 2\epsilon)^{1/2}} ds$$

Let $\psi(0) = \eta_\epsilon$. Then $\psi_\epsilon : [0,1] \to [0, \eta_\epsilon]$. Clearly $\psi_\epsilon^{-1} : [0, \eta_\epsilon] \to [0,1]$ is continuous. Define

$$\phi_\epsilon(t) = \begin{cases} 1 & \text{if } t < 0, \\ \psi_\epsilon^{-1}(t) & \text{if } 0 \le t \le \eta_\epsilon, \\ 0 & \text{if } t > \eta_\epsilon. \end{cases}$$

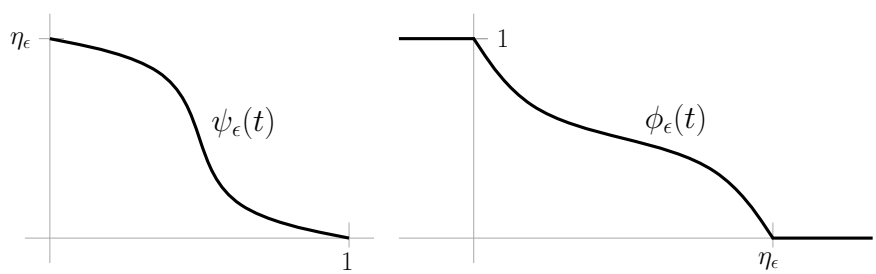

Figure 2.1: Sketches of the functions $\psi_\epsilon(t)$ and $\phi_\epsilon(t)$.

By construction of $\psi_\epsilon(t)$ and the two facts $(f^{-1})'(b) = 1/f'(a)$ (where b = f(a)) and $W(1-t) = W(t)$, $\phi_\epsilon(t)$ has two nice properties:

$$\frac{\epsilon}{2}\phi_\epsilon'^2(t) = \frac{1}{\epsilon}W(\phi_\epsilon(t)) + 1,$$
$$|\phi_\epsilon'(t)| = -\frac{1}{\epsilon}\left(2W(\phi_\epsilon(t)) + 2\epsilon\right)^{1/2}.$$

Note that $\phi_\epsilon(t)$ is a Lipschitz continuous function on $\mathbb{R}$ and that for every $t \in \mathbb{R}$, $\phi_\epsilon(t) \ge \chi_0(t)$ and $\phi_\epsilon(t + \eta_\epsilon) \le \chi_0(t)$. Thus there is $\delta_\epsilon \in [0, \eta_\epsilon]$ s.t.

$$\int_\Omega \phi_\epsilon(d(x) + \delta_\epsilon)dx = \int_\Omega \chi_0(d(x))dx = \int_\Omega \chi_A(x)dx.$$

Define $u_\epsilon = \phi_\epsilon(d(x) + \delta_\epsilon)$.

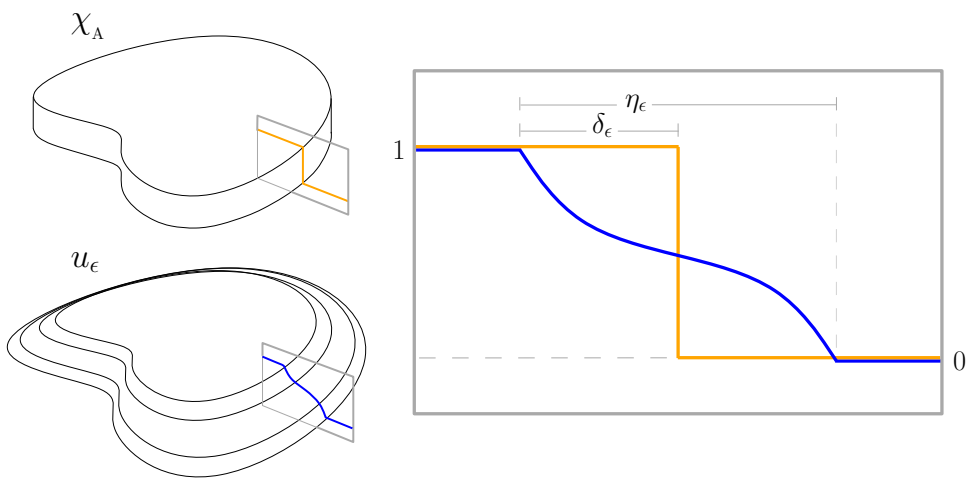

Figure 2.2: 2D comparison of u_ϵ and the characteristic function limit.

Now to show $u_\epsilon \to \chi_A$ in $L^1(\Omega)$. A useful lemma:

Lemma 2.2.3 (Lemma 4 from Modica [26])**.** *Let $A \subset \Omega$ be open, non-empty, and Lebesgue measurable with ∂A Lipschitz continuous and $|dist(A, \partial\Omega)| > 0$. Define*

$$S_t = \{x \in \Omega \mid d(x) = t\}. \tag{2.6}$$

Then $d(x)$ (equation (2.5)) is Lipschitz continuous, $|Dd(x)| = 1$ for almost all $x \in \mathbb{R}^n$, and

$$\lim_{t\to 0} \mathcal{H}_{n-1}(S_t) = \mathcal{H}_{n-1}(\partial A).$$

By this lemma we get:

$$\int_\Omega |u_\epsilon - \chi_A| dx = \int_\Omega |\chi_\epsilon(d(x)) - \chi_0(d(x))||Dh(x)| dx.$$

By the coarea formula (Lemma 2.2.1), the previous expression becomes

$$\begin{aligned} &\int_{\mathbb{R}} |\chi_\epsilon(t) - \chi_0(t)| \mathcal{H}_{n-1}(S_t) dt \\ &= \int_{-\delta_\epsilon}^{\eta_\epsilon - \delta_\epsilon} |\chi_\epsilon(t) - \chi_0(t)| \mathcal{H}_{n-1}(S_t) dt \\ &\leq \eta_\epsilon \sup_{|t| \leq \eta_\epsilon} \mathcal{H}_{n-1}(S_t), \end{aligned} \tag{2.7}$$

where $\mathcal{H}_{n-1}(W)$ denotes the (n-1)-dimensional Hausdorff measure on W. Let

$$\gamma_\epsilon \equiv \sup_{|t| \leq \eta_\epsilon} \mathcal{H}_{n-1}(S_t).$$

Clearly by Lemma 2.2.3

$$\lim_{\epsilon\to 0}\gamma_\epsilon = \mathcal{H}_{n-1}(\partial A), \tag{2.8}$$

so the right hand side of (2.7) approaches 0 as $\epsilon \to 0$ forcing convergence.

It remains to prove the estimate:

$$E_\epsilon[u_\epsilon] = \int_\Omega \frac{\epsilon}{2}|\nabla u_\epsilon|^2 + \frac{1}{\epsilon}W(u_\epsilon)dx. \tag{2.9}$$

By the coarea formula (Lemma 2.2.1),

$$\begin{aligned}
E_\epsilon[u_\epsilon] &= \int_{\mathbb{R}} \left[\frac{\epsilon}{2}\phi_\epsilon'^2(t+\delta_\epsilon) + \frac{1}{\epsilon}W(\phi_\epsilon(t+\delta_\epsilon))\right] \mathcal{H}_{n-1}(\{x\in\Omega : h(x)=t\})dt \\
&\le \gamma_\epsilon \int_{\delta_\epsilon}^{\eta_\epsilon-\delta_\epsilon} \frac{\epsilon}{2}\phi_\epsilon'^2(t+\delta_\epsilon) + \frac{1}{\epsilon}W(\phi_\epsilon(t+\delta_\epsilon))dt \\
&= \gamma_\epsilon \int_0^{\eta_\epsilon} \frac{\epsilon}{2}\phi_\epsilon'^2(t) + \frac{1}{\epsilon}W(\phi_\epsilon(t))dt \\
&\le \gamma_\epsilon \int_0^{\eta_\epsilon} \frac{\epsilon}{2}\phi_\epsilon'^2(t) + \frac{1}{\epsilon}\left(W(\phi_\epsilon(t)) + \epsilon\right)dt \\
&\le \gamma_\epsilon \int_0^{\eta_\epsilon} \frac{1}{2}\phi_\epsilon'(t)\left[2W(\phi_\epsilon'(t)) + 2\epsilon\right]^{1/2} + \left[W(\phi_\epsilon(t)) + \epsilon\right]^{1/2}\frac{\phi_\epsilon'(t)}{2^{1/2}}dt \\
&= \sqrt{2}\gamma_\epsilon \int_0^{\eta_\epsilon} \left[W(\phi_\epsilon(t)) + \epsilon\right]^{1/2}\phi_\epsilon'(t)dt \\
&= \sqrt{2}\gamma_\epsilon \int_0^1 \left(W(s)+\epsilon\right)^{1/2} ds.
\end{aligned}$$

Now take the lim sup.

$$\begin{aligned}
\limsup_{\epsilon\to 0} E_\epsilon[u_\epsilon] &\le \sqrt{2}\limsup_{\epsilon\to 0}\left[\gamma_\epsilon \int_0^1 \left(W(s)+\epsilon\right)^{1/2} ds\right] \\
&= \sqrt{2}\,\mathcal{H}_{n-1}(\partial A)\int_0^1 W(s)^{1/2}ds \\
&= \sqrt{2}\,c_0\,\mathcal{H}_{n-1}(\partial A) \\
&= \sqrt{2}\,c_0\,P_\Omega(A).
\end{aligned}$$

□

2.3 Convergence of Minimizers

Now that we have the existence of minimizers (Theorem 2.1.1) and Gamma-convergence (Theorem 2.2.1) we want to show that that minimizers of the phase field model converge to minimizers of sharp interface functional (Theorem 2.3).

Theorem 2.3.1. *Let $S = \{\chi_B : B \subset \Omega,\ B$ is Lebesgue measurable$\}$. Given $E_0 : S \to \mathbb{R}^+$ and $E_\epsilon : L^1(\Omega) \to \mathbb{R}^+$ as defined in Theorem 2.2.1. Let $u_\epsilon \in H_0^1(\Omega)$ be such that $E_\epsilon[u_\epsilon] = \min_{v \in L^1} E_\epsilon[v]$ for fixed ϵ.*

1. *There exists χ_B, a minimizer of E_0 over S with $u_\epsilon \to \chi_B$ in $L^1(\Omega)$.*
2. *For any $\chi_B \in S$, there exists a subsequence of u_ϵ, call it u_{ϵ_k}, such that $E_0[\chi_B] = \lim_{k\to\infty} E_{\epsilon_k}[u_{\epsilon_k}]$.*

We introduce the following two lemmas before proving Theorem 2.3.

Lemma 2.3.1 (Lemma 2 from Modica [26])**.** *Let Ω be an open, bounded subset of $\mathbb{R}^n$ with Lipschitz continous boundary, and let E be a measurable subset of Ω with $0 < |E| < |\Omega|$. If for a fixed $\lambda > 0$ we have $\lambda \leq P_\Omega(A)$ for every open, bounded subset A with smooth boundary and satisfying $\mathcal{H}_{n-1}(\partial A \cap \partial\Omega) = 0$, $|A \cap \Omega| = |E|$, then*

$$\lambda \leq \min\{P_\Omega(F) :\ F \text{ measurable subset of } \Omega,\ |F| = |E|\}$$

If, in particular, $\lambda = P_\Omega(E)$, then equality holds.

Lemma 2.3.2 (Proposition 3 from Modica [26])**.** *Suppose u_ϵ minimizes E_ϵ for every $\epsilon > 0$ and suppose there exists $t_0 > 0$, $c_1 > 0$, $c_2 > 0$ such that*

$$c_1 t^4 \leq W(t) \leq c_2 t^4 \qquad \forall\, t \geq t_0.$$

Then there exists a sequence $\{\epsilon_k\}$ of positive numbers such that $\epsilon_k \to 0$ and $\{u_{\epsilon_k}\}$ converges to u_0 in $L^1(\Omega)$ as $k \to \infty$.

Proof of Lemma 2.3.2. See proof in Modica [26]. The energy E_ϵ here has one more term than the energy functional in Modica's paper but for the sake of the proof that doesn't matter. □

Proof of Theorem 2.3. The proof has two parts:

1. Prove a subsequence of minimizers of E_ϵ, $\{u_\epsilon\}$, converges in $L^1(\Omega)$ to a minimum of E_0.

2. Prove the energy of the minimizers converges up to a subsequence to the energy of the limit, i.e. $\lim_{\epsilon\to 0} E_\epsilon[u_{\epsilon_k}] = E_0[u_0]$.

Consider part (1) of Theorem . By Lemma 2.3.2 there exists, passing to a subsequence if necessary, a $u_0 = \lim_{\epsilon\to 0} u_\epsilon$ where $\{u_\epsilon\}$ is the sequence of minimizers:

$$\lim_{\epsilon\to 0} E_\epsilon[u_\epsilon] = \lim_{\epsilon\to 0} \inf_{L^1} E_\epsilon.$$

$u_0 = \chi_B$ for some B otherwise the double well potential makes the energy go to infinity. Let A be a set with Lipschitz boundary and v_ϵ the sequence corresponding to A as constructed in Proposition 2.2. Observe the following inequality.

$$\lambda := E_0[\chi_B] \overset{(1)}{\leq} \liminf_{\epsilon\to 0} E_\epsilon[u_\epsilon] \overset{(2)}{\leq} \limsup_{\epsilon\to 0} E_\epsilon[u_\epsilon] \overset{(3)}{\leq} \limsup_{\epsilon\to 0} E_\epsilon[v_\epsilon] \overset{(4)}{\leq} E_0[\chi_A]$$

1. Liminf inequality (Theorem 2.2.1 Part 1).

2. Follows trivially from definition of infimum and supremum.

3. Since u_ϵ is minimizer of E_ϵ, $E_\epsilon[u_\epsilon] \leq E_\epsilon[v_\epsilon]\ \forall\ v_\epsilon$.

4. Limsup inequality (Theorem 2.2.1 Part 2)

Since $E_0[\chi_A] = P_\Omega(A) \geq \lambda$ for all A with Lipschitz continuous boundary such that $|A| = |B| = V$, by Lemma 2.3.1,

$$\begin{aligned}\inf_S E_0 &= \min\{P_\Omega(F) :\ |F| = |A| = V\}\\ &= \lambda = E_0[\chi_B].\end{aligned}$$

Thus χ_B is a minimizer for the sharp interface functional.

Consider part (2) of Theorem . Given the following inequality, it suffices to prove (5).

$$\begin{aligned}\inf_S E_0 = E_0[\chi_B] \leq \liminf_{\epsilon\to 0} E_\epsilon[u_\epsilon] &\leq \limsup_{\epsilon\to 0} E_\epsilon[u_\epsilon]\\ &\leq \limsup_{\epsilon\to 0} E_\epsilon[v_\epsilon] \leq E_0[\chi_A] \overset{(5)}{\leq} \inf_S E_0.\end{aligned}$$

(5) By Lemma 2.3.1, for any $\delta > 0$, it is possible to choose A with Lipschitz boundary such that

$$E_0[\chi_A] \leq \inf_S E_0 + \delta.$$

Thus there exists a sequence of $\delta_n \to 0$ and corresponding A_n such that

$$E_0[\chi_{A_n}] \leq \inf_S E_0 + \delta_n.$$

By arbitrariness of δ_n,

$$\inf_S E_0 \leq \liminf_{\epsilon \to 0} E_\epsilon[u_\epsilon] \leq \limsup_{\epsilon \to 0} E_\epsilon[u_\epsilon] \leq \inf_S E_0$$

and $\inf_S E_0 = \lim_{\epsilon \to 0} E_\epsilon[u_\epsilon] = E_0[\chi_B]$.

$\square$

Chapter 3

The Shao–Rappel–Levine Energy Functional: Including H^2

We now begin work on the 3-term Shao–Rappel–Levine functional, labeled $\mathcal{E}$ instead of E to distinguish it from the previous 2-term functional.

Definition 3.1. The set of smooth characteristic functions: Let S^* be the collection of characteristic functions χ_A of sets $A \subset \Omega$ where A is open and non-empty, ∂A is C^2 continuous, and $|dist(A, \partial\Omega)| > 0$.

Definition 3.2. The H^2 functionals, $\mathcal{E}_0 : S^* \to \mathbb{R}^+ \cup \infty$ and $\mathcal{E}_\epsilon : L^1(\Omega) \to \mathbb{R}^+ \cup \infty$.

$$\mathcal{E}_0[\chi_A] = \begin{cases} \sqrt{2}c_0 \left(\mathcal{H}_{n-1}(\partial A) + \int_{\partial A} |\mathbf{H}_{\partial A}|^2 d\mathcal{H}_{n-1} \right) & \text{if } \int \chi_A dx = V, \\ \infty & \text{if } \int \chi_A dx \neq V. \end{cases}$$

$$\mathcal{E}_\epsilon[u] = \begin{cases} \int_\Omega \left[\frac{\epsilon}{2} |\nabla u|^2 + \frac{1}{\epsilon} W(u) \right] dx + M(\epsilon) \left(\int_\Omega u \, dx - V \right)^2 & \\ + \int_\Omega \frac{1}{\epsilon} \left[-\epsilon \Delta u + \frac{W'(u)}{\epsilon} \right]^2 dx & \text{if } u \in H_0^2(\Omega), \\ \infty & \text{if } u \in L^1(\Omega) \backslash H_0^2(\Omega). \end{cases}$$

3.1 Existence of Minimizers

Theorem 3.1.1. *Fix ϵ and let $\mathcal{E}_\epsilon$ be defined as in Definition 3.2. There exists $u \in H_0^2(\Omega)$ such that*

$$0 \leq \mathcal{E}_\epsilon[u] = \min_{v \in L^1(\Omega)} \mathcal{E}_\epsilon[v] < \infty.$$

Proof of Theorem 3.1.1. Let

$$\alpha = \inf_{v \in L^1(\Omega)} \mathcal{E}_\epsilon[v].$$

Since $\mathcal{E}_\epsilon[v] \geq 0$ for all $v \in L^1(\Omega)$, $\alpha \geq 0$. If $v(x) \equiv 0$ $\forall x \in \Omega$, then $\mathcal{E}_\epsilon[v] = M(\epsilon)V^2 > 0$. Thus, $\alpha \leq \mathcal{E}_\epsilon[v] < \infty$. Let $\{u_k\} \subset L^1(\Omega)$ be a sequence such that

$$\mathcal{E}_\epsilon[u_k] \to \alpha.$$

This implies that $\mathcal{E}_\epsilon[u_k]$ is finite for $k \geq k_0$ for some k_0. Therefore, we may assume that, without loss of generality, that all $\mathcal{E}_\epsilon[u_k]$ $(k = 1,2,...)$ are finite. Hence $u_k \in H_0^2(\Omega)$ by the definition of $\mathcal{E}_\epsilon[\cdot]$. Pick a $C_0 > \alpha$ and k_0 such that for $k \geq k_0$,

$$C_0 > \mathcal{E}_\epsilon[u_k].$$

The goal now is to show that this sequence is bounded in the $H_0^2(\Omega)$ norm by which we can extract a convergent subsequence. To do this we need the following theorem and lemmas.

Theorem 3.1.2 (Theorem 5.6.3 of Evans [14])**.** *Let Ω be bounded domain in $\mathbb{R}^3$. Let $1 \leq q \leq 6$. Then there exists a constant C_1 such that:*

$$C_1 \|u\|_{H_0^1} \geq \|u\|_{L^q} \qquad \forall\, u \in H_0^1(\Omega)$$

Lemma 3.1.1. *Assume $\mathcal{E}_\epsilon[u_k]$ is bounded. Then $\|u_k\|_{H_0^1(\Omega)}$ is bounded.*

Proof of Lemma 3.1.1. By definition of $\mathcal{E}_\epsilon[u_k]$, there exists a C_2 such that

$$C_0 > \mathcal{E}_\epsilon[u_k] \geq C_2 \|\nabla u_k\|_{L^2(\Omega)}.$$

By Poincure inequality we get, for some C_3,

$$\|\nabla u_k\|_{L^2(\Omega)} \geq C_3 \|u_k\|_{L^2(\Omega)}.$$

Thus there exists a C_4 such that

$$C_4 > \|u_k\|_{H_0^1(\Omega)}.$$

□

Lemma 3.1.2. *Assume $\mathcal{E}_\epsilon[u_k]$ is bounded. Then $\int_\Omega |\Delta u_k|^2\,dx$ is bounded.*

Proof of Lemma 3.1.2. By assumption and definition of $\mathcal{E}_\epsilon[u_k]$,

$$\begin{aligned} C_0 &> \mathcal{E}_\epsilon[u_k] \\ &\geq \int_\Omega \frac{1}{\epsilon}\left[-\epsilon\Delta u_k + \frac{W'(u_k)}{\epsilon}\right]^2 dx \\ &\geq \epsilon\int_\Omega |\Delta u_k|^2\,dx - \frac{2}{\epsilon}\int_\Omega W'(u_k)\Delta u_k\,dx + \frac{1}{\epsilon^3}\int_\Omega |W'(u_k)|^2\,dx. \end{aligned} \tag{3.1}$$

Looking at the middle term we use the fact that $2ab \leq \frac{1}{\delta}a^2 + \delta b^2$ to get

$$\frac{2}{\epsilon}\int_\Omega W'(u_k)\Delta u_k\,dx \leq \frac{1}{\delta\epsilon}\int_\Omega |W'(u_k)|^2\,dx + \frac{\delta}{\epsilon}\int_\Omega |\Delta u_k|^2\,dx, \tag{3.2}$$

and then substitute this into the above inequality (3.1) to get

$$C_0 > \left(\epsilon - \frac{\delta}{\epsilon}\right)\int_\Omega |\Delta u_k|^2\,dx + \left(\frac{1}{\epsilon^3} - \frac{1}{\delta\epsilon}\right)\int_\Omega |W'(u_k)|^2\,dx.$$

Moving the W' term to the left side of the inequality and choosing $\delta < \epsilon^2$ so that $C_5 \equiv \left(\frac{1}{\delta\epsilon} - \frac{1}{\epsilon^3}\right) > 0$ and $C_6 \equiv \left(\epsilon - \frac{\delta}{\epsilon}\right) > 0$, we get

$$C_0 + C_5\int_\Omega |W'(u_k)|^2\,dx > C_6\int_\Omega |\Delta u_k|^2\,dx. \tag{3.3}$$

Noticing that the powers of u in $W'(u)^2$ are less than or equal to 6, we can apply Theorem 3.1.2 and Lemma 3.1.1 to bound the left hand side of (3.3):

$$\begin{aligned} C_0 + C_4C_1C_5 &> C_0 + C_1C_5\|u_k\|_{H_0^1} && \text{(Lemma 3.1.1)} \\ &\geq C_0 + C_5\int_\Omega |W'(u_k)|^2\,dx && \text{(Theorem 3.1.2)} \\ &> C_6\int_\Omega |\Delta u_k|^2\,dx. && (3.4) \end{aligned}$$

So, for fixed ϵ, the sequence $\left\{\int_\Omega |\Delta u_k|^2\,dx\right\}_{k=1}^\infty$ is bounded. □

Lemma 3.1.3. *If $\|u_k\|_{H_0^1(\Omega)}$ and $\int_\Omega |\Delta u_k|^2\,dx$ are bounded, then $\|u_k\|_{H_0^2(\Omega)}$ is bounded.*

Proof of Lemma 3.1.3. It suffices to prove a bound on the second derivative terms:

$$\begin{aligned}\int_\Omega (\partial_i\partial_j u_k)^2 dx &= \int_\Omega (\partial_i\partial_j u_k)(\partial_i\partial_j u_k)\,dx \\ &= -\int_\Omega (\partial_j u_k)(\partial_i^2\partial_j u_k)\,dx + \int_{\partial\Omega} \frac{\partial u_k}{\partial n}\partial_i\partial_j u_k\,dx' \\ &= \int_\Omega (\partial_j^2 u_k)(\partial_i^2 u_k)\,dx \\ &= \int_\Omega |\Delta u_k|^2\,dx < C.\end{aligned}$$

□

Since $\{u_k\}_{k=1}^\infty$ is bounded in $H_0^2(\Omega)$, by compact embedding, it has a subsequence not relabeled such that, for some $u \in H_0^2(\Omega)$,

$$u_k \rightharpoonup u \text{ in } H_0^2(\Omega),$$

$$u_k \to u \text{ a.e. } \Omega,$$

$$u_k \to u \text{ in } L^q(\Omega) \quad \text{for } q < 6.$$

Given $\liminf_{k\to\infty} E_\epsilon[u_k] \geq E_\epsilon[u]$ from the proof of Theorem 2.1.1, if suffices to show

$$\liminf_{k\to\infty} \int_\Omega \frac{1}{\epsilon}\left[-\epsilon\Delta u_k + \frac{W'(u_k)}{\epsilon}\right]^2 dx \geq \int_\Omega \frac{1}{\epsilon}\left[-\epsilon\Delta u + \frac{W'(u)}{\epsilon}\right]^2 dx. \tag{3.5}$$

Expanding the this term we get:

$$\begin{aligned}\int_\Omega \frac{1}{\epsilon}\left[-\epsilon\Delta u_k + \frac{W'(u_k)}{\epsilon}\right]^2 dx = \epsilon\int_\Omega (\Delta u_k)^2\,dx - \frac{1}{\epsilon}\int_\Omega 2\Delta u_k W'(u_k)\,dx \\ + \frac{1}{\epsilon^3}\int_\Omega W'(u_k)^2\,dx.\end{aligned}$$

We establish equation (3.5) by showing the liminf bound for each of these three terms:

Bounding the Laplace Term

We want to show

$$\liminf_{k\to\infty} \epsilon \int_\Omega (\Delta u_k)^2\,dx \geq \epsilon \int_\Omega (\Delta u)^2\,dx.$$

Since

$$0 \leq \int_\Omega (\Delta u_k - \Delta u)^2\,dx = \int_\Omega (\Delta u_k)^2\,dx - 2\int_\Omega \Delta u_k \Delta u\,dx + \int (\Delta u)^2\,dx,$$

we get

$$\int_\Omega (\Delta u_k)^2\,dx \geq 2\int_\Omega \Delta u_k \Delta u\,dx - \int (\Delta u)^2\,dx.$$

Taking the lim inf and using the fact that u_k converges weakly to u in $H^2(\Omega)$ we get:

$$\begin{aligned}\liminf_{k\to\infty} \int_\Omega (\Delta u_k)^2\,dx &\geq \liminf_{k\to\infty} 2\int_\Omega \Delta u_k \Delta u\,dx - \int (\Delta u)^2\,dx \\ &= 2\int_\Omega \Delta u \Delta u\,dx - \int_\Omega (\Delta u)^2\,dx \\ &= \int_\Omega (\Delta u)^2\,dx.\end{aligned}$$

Bounding the Potential Term

We want to show

$$\liminf_{k\to\infty} \frac{1}{\epsilon^3} \int_\Omega W'(u_k)^2\,dx \geq \frac{1}{\epsilon^3} \int_\Omega W'(u)^2\,dx.$$

Fatou's Lemma implies that

$$\int_\Omega W'(u)^2\,dx = \int_\Omega \lim_{k\to\infty} W'(u_k)^2\,dx \leq \liminf_{k\to\infty} \int_\Omega W'(u_k)^2\,dx.$$

Bounding the Cross Term

We want to show

$$\liminf_{k\to\infty} \frac{1}{\epsilon} \int_\Omega -2\Delta u_k W'(u_k)\,dx \geq \frac{1}{\epsilon} \int_\Omega -2\Delta u W'(u)\,dx.$$

Let $M \in \mathbb{R}^+$ be such that $W''(t) + M > 0$ for all t.

$$\begin{aligned}
\int_\Omega -\Delta u_k W'(u_k)\,dx &= \int_\Omega \nabla u_k \cdot \nabla(W'(u_k))\,dx - \int_{\partial\Omega} \frac{\partial u_k}{\partial n} W'(u_k)\,dx' \\
&= \int_\Omega \nabla u_k \cdot (W''(u_k)\nabla u_k)\,dx \\
&= \int_\Omega |\nabla u_k|^2 W''(u_k)\,dx \\
&= \int_\Omega |\nabla u_k|^2 (W''(u_k) + M)\,dx - \int_\Omega |\nabla u_k|^2 M\,dx.
\end{aligned}$$

Now, $\nabla u_k \to \nabla u$ strongly. Additionally, $|\nabla u_k|^2(W''(u_k) + M) \geq 0$ and converges to $|\nabla u|^2(W''(u)+M)$ pointwise. Thus, by Fatou's Lemma and strong convergence:

$$\begin{aligned}
\liminf_{k\to\infty} \int_\Omega -\Delta u_k W'(u_k)\,dx &= \liminf_{k\to\infty} \left[\int_\Omega |\nabla u_k|^2 (W''(u_k) + M)\,dx - \int_\Omega |\nabla u_k|^2 M\,dx\right] \\
&\geq \int_\Omega |\nabla u|^2 (W''(u) + M)\,dx - \int_\Omega |\nabla u|^2 M\,dx \\
&= \int_\Omega |\nabla u|^2 W''(u)\,dx.
\end{aligned}$$

Having bounded all three terms, we establish equation 3.5 and

$$\alpha = \liminf_{k\to\infty} \mathcal{E}_\epsilon[u_k] \geq \mathcal{E}_\epsilon[u] \geq \alpha.$$

□

3.2 Gamma-Convergence and Convergence of Minimizers

Our goal in this section is to prove the following theorem.

Theorem 3.2.1. *Let $\mathcal{E}_\epsilon$ and $\mathcal{E}_0$ be defined as in Definition 3.2.*

1. *Let $\{u_\epsilon\}$ be any sequence of functions in $H_0^2(\Omega)$ such that $u_\epsilon \to \chi_A$ in $L^1(\Omega)$. Then*

$$\liminf_{\epsilon\to 0} \mathcal{E}_\epsilon[u_\epsilon] \geq \mathcal{E}_0[\chi_A] \tag{3.6}$$

2. *For any $A \subseteq \Omega$ open and non-empty with C^2-continuous ∂A and $|dist(A, \partial\Omega)| > 0$, there exists $u_\epsilon \to \chi_A$ in L^1 such that*

$$\limsup_{\epsilon \to 0} \mathcal{E}_\epsilon[u_\epsilon] \leq \mathcal{E}_0[\chi_A] \tag{3.7}$$

3.2.1 Proof of Theorem 3.3: Part 1

Proof. Roger and Schätzle [28] show that $\mathcal{F}_\delta$ Gamma-converges to $\mathcal{F}_0$ in the following theorem. We relate $\mathcal{E}_\epsilon$, $\mathcal{E}_0$ to $\mathcal{F}_\delta$, $\mathcal{F}_0$ and use this theorem in proving Gamma-convergence of $\mathcal{E}_\epsilon$ to $\mathcal{E}_0$.

Theorem 3.2.2 (Theorem 1.2 of Roger and Schätzle [28])**.** *Let*

$$\mathcal{F}_0[\chi] = \sigma \left[\mathcal{H}_{n-1}(\partial A) + \int_{\partial A} |\boldsymbol{H}_{\partial A}|^2 d\mathcal{H}_{n-1} \right]$$

$$\mathcal{F}_\delta[v] = \begin{cases} \int_\Omega \left[\frac{\delta}{2} |\nabla v|^2 + \frac{1}{\delta} W_r(v) \right] dx + \int_\Omega \frac{1}{\delta} \left[-\delta \Delta v + \frac{W_r'(v)}{\delta} \right]^2 dx & \text{if } v \in H_0^2(\Omega) \\ \infty & \text{if } v \in L^1(\Omega) \backslash H_0^2(\Omega) \end{cases}$$

with double welled potential $W_r(t) = (1-t^2)^2$, $\chi = 2\chi_A - 1$, and $\sigma = \int_{-1}^{1} \sqrt{2W_r(t)}\, dt$. For any χ where $A \subset \Omega$ and $\partial A \cap \Omega \in C^2$,

$$\mathcal{F}_\delta \text{ Gamma-converges to } \mathcal{F}_0 \text{ in } L^1(\Omega) \text{ as } \delta \to 0.$$

Relating the quantities in $\mathcal{F}_\delta$, $\mathcal{F}_0$ to the quantities in $\mathcal{E}_\epsilon$, $\mathcal{E}_0$:

$$W_r(t) = 16W\left(\tfrac{1}{2}(t+1)\right), \quad v = 2u - 1, \quad \delta = 2\epsilon,$$

these functionals become

$$\mathcal{F}_0[2\chi_A - 1] = 8\sqrt{2}c_0 \left[\mathcal{H}_{n-1}(\partial A) + \int_{\partial A} |\mathbf{H}_{\partial A}|^2 d\mathcal{H}_{n-1} \right],$$

$$\mathcal{F}_{2\epsilon}[2u - 1] = 8 \int_\Omega \left[\frac{\epsilon}{2} |\nabla u|^2 + \frac{1}{\epsilon} W(u) \right] dx + \int_\Omega \frac{1}{\epsilon} \left[-\epsilon \Delta u + \frac{W'(u)}{\epsilon} \right]^2 dx.$$

Assume $\int \chi_A dx = V$. If $u_\epsilon \xrightarrow{L^1} \chi_A$ then $v_\epsilon \xrightarrow{L^1} \chi$ and, via the Γ-convergence

of $\mathcal{F}_\delta \to \mathcal{F}_0$, we get

$$\begin{aligned}
\mathcal{E}_0[\chi_A] &= \sqrt{2}c_0 \left[\mathcal{H}_{n-1}(\partial A) + \int_{\partial A} |\mathbf{H}_{\partial A}|^2 d\mathcal{H}_{n-1} \right] \\
&\leq \liminf_{\epsilon \to 0} \left[\int_\Omega \left[\frac{\epsilon}{2} |\nabla u_\epsilon|^2 + \frac{1}{\epsilon} W(u_\epsilon) \right] dx + \int_\Omega \frac{1}{\epsilon} \left[-\epsilon \Delta u_\epsilon + \frac{W'(u_\epsilon)}{\epsilon} \right]^2 dx \right] \\
&\leq \liminf_{\epsilon \to 0} \mathcal{E}_\epsilon[u_\epsilon].
\end{aligned}$$

If $\int \chi_A dx \neq V$ then $\mathcal{E}_0[\chi_A] = \infty$ and since $\int u_\epsilon \, dx \to \int \chi_A dx \neq V$:

$$\liminf_{\epsilon \to 0} M(\epsilon) \left(\int_\Omega u_\epsilon \, dx - V \right)^2 = \infty,$$

and the inequality is trivial. □

3.2.2 Proof of Theorem 3.3: Part 2

Proof. To prove part 2, we need to construct a sequence $u_\epsilon \to \chi_A$ in $L^1(\Omega)$ such that

$$\limsup_{\epsilon \to 0} \mathcal{E}_\epsilon[u_\epsilon] \leq \mathcal{E}_0[\chi_A].$$

In this proof, we assume $\int \chi_A dx = V$. Otherwise, by the same argument as just presented in the proof of Part 1, both sides are ∞ and the inequality is trivial.

To begin construction of this sequence, define

$$\Gamma_\epsilon(t) := \begin{cases} \gamma(t) & \text{if } 0 \leq t < t_\epsilon \\ p_\epsilon(t) & \text{if } t_\epsilon < t < 2t_\epsilon \\ 1 & \text{if } t > 2t_\epsilon \\ -\Gamma_\epsilon(-t) & \text{if } t < 0 \end{cases}$$

where $t_\epsilon = \epsilon \log \epsilon$, $\gamma(t) = \tanh(t)$, and $p_\epsilon(t)$ is some third degree polynomial constructed so that $\Gamma_\epsilon(t)$ is $C^1(\mathbb{R})$.

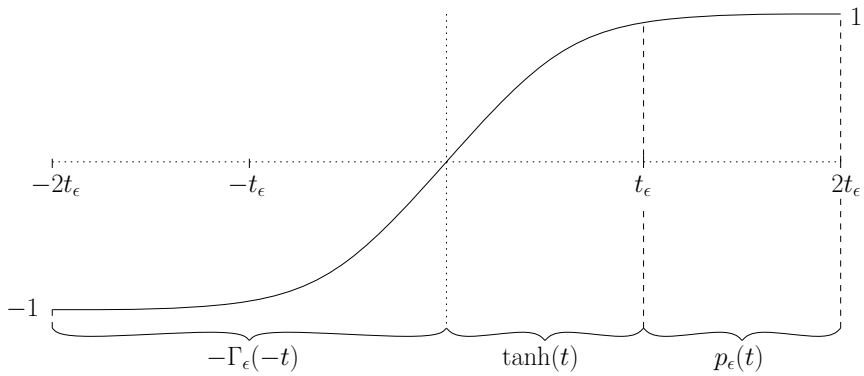

Figure 3.1: Sketch of Γ_ϵ.

Now let

$$u_\epsilon(x) = \frac{1}{2}\left(\Gamma_\epsilon\left(\frac{-d(x)}{\epsilon}\right) + 1\right),$$

where

$$d(x) = \begin{cases} -\mathrm{dist}(x, \partial A) & \text{if } x \in A, \\ \mathrm{dist}(x, \partial A) & \text{if } x \notin A. \end{cases}$$

Figure 3.2 illustrates both χ_A and u_ϵ; note that they differ only on the band $\{x \in \mathbb{R}^n | \ \mathrm{dist}(x, \partial A) \leq 2t_\epsilon\}$.

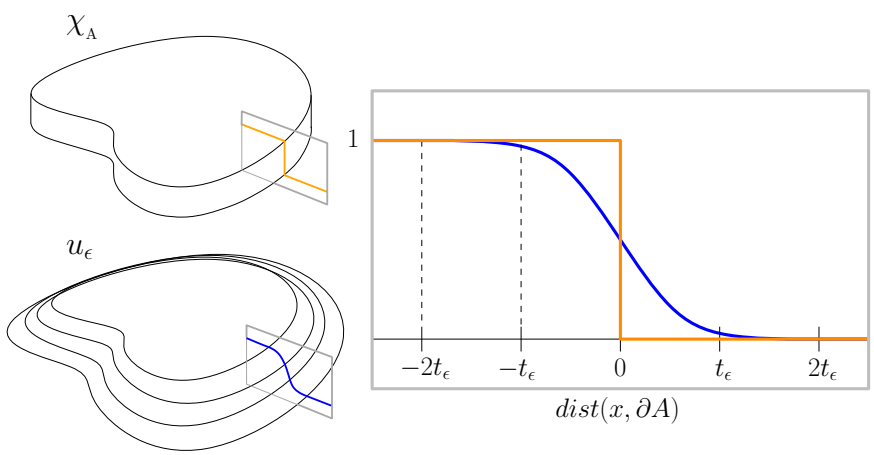

Figure 3.2: Comparison of χ_A and u_ϵ.

Bellettini [3] proved that with this sequence the inequality holds for the

bending (H^2) term and surface area terms. Thus, it suffices to show that

$$\limsup_{\epsilon\to 0} M(\epsilon)\left(\int_\Omega u_\epsilon dx - V\right)^2 = 0.$$

Since ∂A is smooth, $\chi_A = \chi_0(d(x))$. By Lemma 2.2.3 we get

$$\int_\Omega |u_\epsilon - \chi_A| dx = \int_\Omega |\chi_\epsilon(d(x)) - \chi_0(d(x))||Dd(x)|dx.$$

By the coarea formula (Lemma 2.2.1):

$$\begin{aligned}\int_\Omega |\chi_\epsilon(d(x)) - \chi_0(d(x))||Dd(x)|dx &= \int_{\mathbb{R}} |\chi_\epsilon(t) - \chi_0(t)|\mathcal{H}_{n-1}(S_t)dt \\ &= \int_{-2t_\epsilon}^{2t_\epsilon} |\chi_\epsilon(t) - \chi_0(t)|\mathcal{H}_{n-1}(S_t)dt \\ &\leq 4t_\epsilon \sup_{|t|\leq 2t_\epsilon} \mathcal{H}_{n-1}(S_t).\end{aligned}$$

Thus,

$$M(\epsilon)\left(\int_\Omega u_\epsilon dx - \int \chi_A dx\right)^2 \leq M(\epsilon)(4t_\epsilon)^2 \sup_{|t|\leq 2t_\epsilon} (\mathcal{H}_{n-1}(S_t))^2$$

By Lemma 2.2.3, for $M(\epsilon) = o\left(\frac{1}{\epsilon}\right)$, the right hand side goes to zero in the $\epsilon \to 0$ limit.

$$\lim_{\epsilon\to 0}\left[M(\epsilon)(4t_\epsilon)^2 \sup_{|t|\leq 2t_\epsilon} (\mathcal{H}_{n-1}(S_t))^2\right] = (0)\cdot(\mathcal{H}_{n-1}(\partial A))^2 = 0.$$

□

3.2.3 Minimizers Converge to Minimizers

By the Theorem 3.1.1 we get existence of minimums u_ϵ. We have only proved the two inequalities for $u_\epsilon \to \chi_A$ where A has "smooth boundary", so we can only establish that minimizers converge to minimizers under the assumption that the minimizers of $\mathcal{E}_\epsilon$ converge to such A with smooth boundary.

Theorem 3.2.3.

Let $\{u_\epsilon\}_{\epsilon>0}$ be the sequence of minimizers of $\mathcal{E}_\epsilon$. Assume the $L^1(\Omega)$-limit of $u_\epsilon \to \chi_{A'}$, has smooth boundary. Then

$$\inf_{S^*} \mathcal{E}_0 = \mathcal{E}_0[\chi_{A'}].$$

Proof. By the assumption, Theorem 3.2.2 part 1 gives us inequality (1). Inequalities (2) and (3) are trivial. Inequality (4) follows from Theorem 3.2.2 part 2.

$$\mathcal{E}_0[\chi_{A'}] \overset{(1)}{\leq} \liminf_{\epsilon\to 0} \mathcal{E}_\epsilon[u_\epsilon] \overset{(2)}{\leq} \limsup_{\epsilon\to 0} \mathcal{E}_\epsilon[u_\epsilon] \overset{(3)}{\leq} \limsup_{\epsilon\to 0} \mathcal{E}_\epsilon[v_\epsilon] \overset{(4)}{\leq} \mathcal{E}_0[\chi_A]$$

We conclude that

$$\inf_{S^*} \mathcal{E}_0 = \mathcal{E}_0[\chi_{A'}].$$

□

Chapter 4

Numerical Simulations

4.1 Finite Difference Method for 3D Radially Symmetric Cells

In this section, we numerically find minimizers of the 2-term functional

$$E_\epsilon[u] = \int_\Omega \left[\frac{\epsilon}{2}|\nabla u|^2 + \frac{1}{\epsilon}W(u)\right] dx + M(\epsilon)\left(\int_\Omega u\,dx - V\right)^2$$

among all radially symmetric phase fields: $u = u(r)$ with $r = |x|$. We use an implicit finite difference method to solve the steepest descent equation:

$$\frac{\partial u}{\partial t} = -\frac{\delta E_\epsilon}{\delta u} = \epsilon u'' + \frac{\epsilon}{2r}u' - \frac{1}{\epsilon}W'(u) - \frac{1}{\epsilon}\left[\int_0^\infty 4\pi r^2 u\,dr - V_0\right].$$

Note that we assume $M(\epsilon) = 1/(2\epsilon)$.

Applying forward difference in time, second order central difference for d^2/dr^2, and backward difference for d/dr, we obtain the linear system of equations:

$$\begin{aligned} u_i^{(n)} &- \frac{\Delta t\epsilon(u_{i+1}^{(n)} - 2u_i^{(n)} + u_{i-1}^{(n)})}{(\Delta r)^2} - \frac{\Delta t\epsilon(u_{i+1}^{(n)} - u_i^{(n)})}{2r\Delta x} \\ &= u_i^{(n-1)} - \frac{\Delta t\, W'(u_i^{(n-1)})}{\epsilon} - \frac{\Delta t}{\epsilon}\left[\sum_{i=1}^N 4\pi r^2 u_i^{(n-1)}\Delta r - 4\pi\right]. \end{aligned}$$

With this system in the form

$$A\mathbf{u}^{(n)} = \mathbf{b},$$

where $\mathbf{b}$ is a function of $\mathbf{u}^{(n-1)}$ and A is the coefficient matrix, we can solve for $\mathbf{u}^{(n)}$ in each time step by inverting A. In our simulation we set the domain to be a sphere of radius 2 and $\Delta r = .004$ so that space is discretized into $N = 500$ concentric circles. We set the initial configuration to (*cf.* Figure 4.1)

$$\mathbf{u}^0 = \frac{1}{2}\tanh\left(\frac{1-2r}{2\epsilon}\right) + \frac{1}{2} + h\cos(2\pi r),$$

where h is a "noise amplitude" parameter that is fixed in each experiment. Finally, we discretize time into steps of size $\Delta t = .001$ and run the program until the energy levels out (*cf.* Figure 4.3).

The results are as expected: $\mathbf{u}^t$ quickly assumes values 1 and 0 for most positions and the transition region moves to $r = 1$. This corresponds to a sphere with an ideal volume of $4/3\pi$.

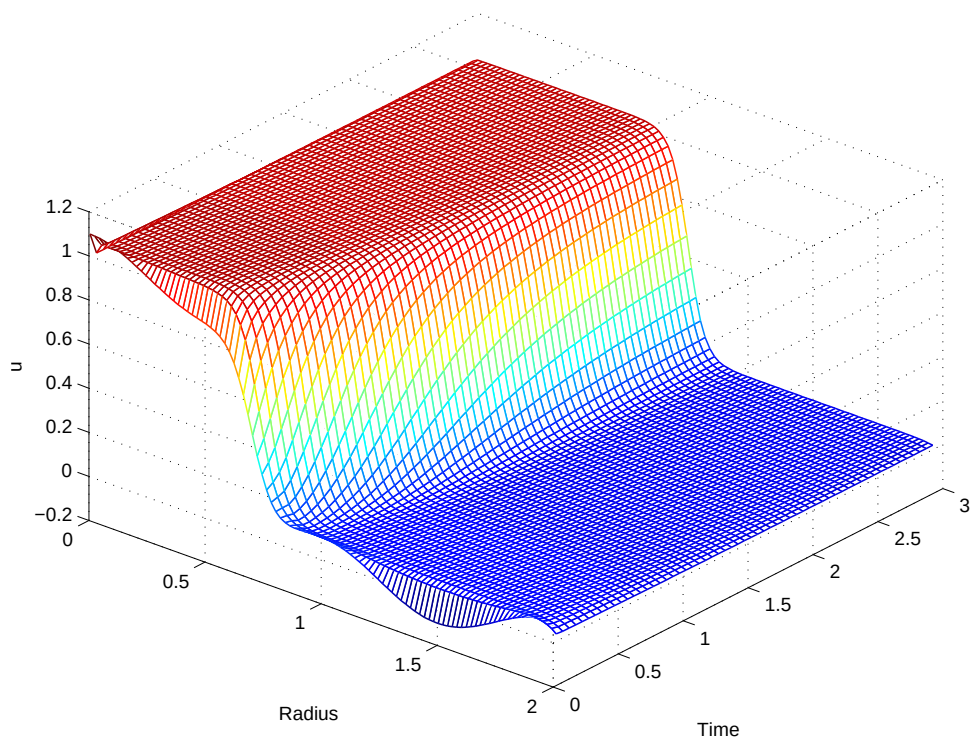

Figure 4.1: The phase field as function of radius and time for $h = .1$

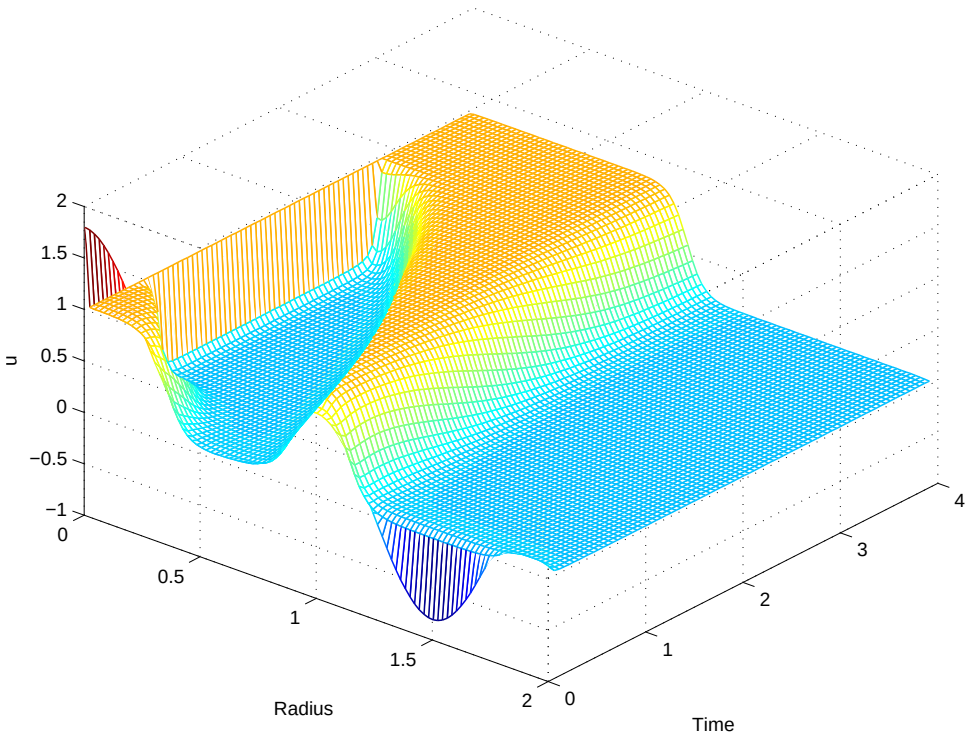

Figure 4.2: The phase field as function of radius and time for $h = .8$.

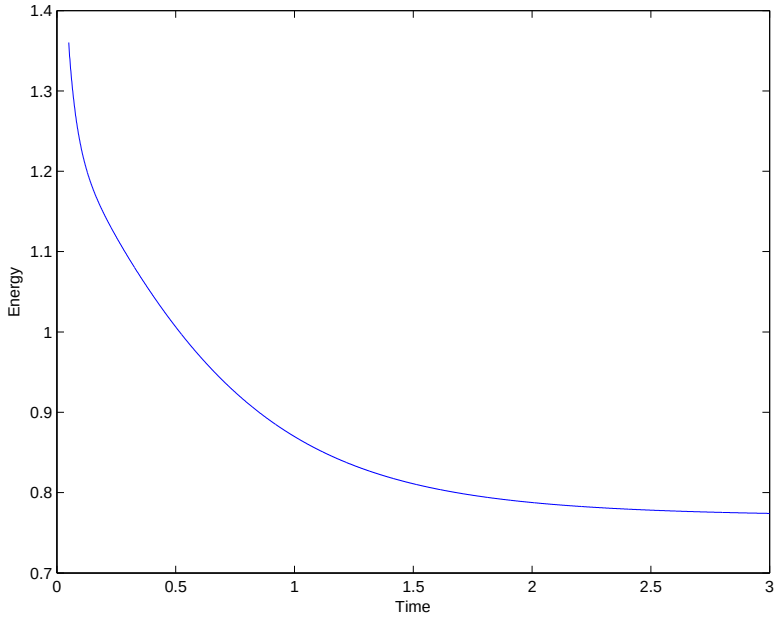

Figure 4.3: Energy of u versus time for experiment with $h = .1$ initial profile .

4.2 2D Simulations Using the Fourier Spectral Method

4.2.1 Schemes

The Shao–Rappel–Levine functional

To find minimums of the the Shao–Rappel–Levine functional,

$$\begin{aligned}\mathcal{E}[u] = &\int_\Omega \left[\frac{\epsilon}{2}|\nabla u|^2 + \frac{1}{\epsilon}W(u)\right] dx + M(\epsilon)\left(\int_\Omega u\, dx - V\right)^2 \\ &+ \int_\Omega \frac{1}{\epsilon}\left[-\epsilon\Delta u + \frac{W'(u)}{\epsilon}\right]^2 dx,\end{aligned}$$

we solve the steepest descent problem

$$\frac{\partial u}{\partial t} = -\frac{1}{\epsilon}\frac{\delta \mathcal{E}}{\delta u}.$$

Here the additional $1/\epsilon$ is the numerical mobility. We discretize this equation using the Semi-Implicit Euler scheme.

The functional derivative of the Shao-Rappel-Levine functional is

$$\begin{aligned}\frac{\delta \mathcal{E}}{\delta u} &= \frac{\partial L}{\partial u} - \nabla\cdot\frac{\partial L}{\partial \nabla u} + \Delta\cdot\frac{\partial L}{\partial \Delta u}. \\ &= \tilde{\kappa}\left[\epsilon\Delta^2 u - \frac{1}{\epsilon}\Delta W'(u) + \frac{1}{\epsilon^3}W'(u)W''(u) - \frac{1}{\epsilon}\Delta u W''(u)\right] \\ &\quad + \gamma\left[-\epsilon\Delta u + \frac{1}{\epsilon}W'(u)\right] + 2M(\epsilon)\left(\int_\Omega u\, dx - A\right).\end{aligned}$$

Here $\tilde{\kappa}$ is a rescaled bending coefficient and $\gamma = 1$ is a scaling parameter. We discretize our steepest descent equation with the following semi-implicit scheme:

$$\begin{aligned}\frac{\partial u}{\partial t} &\to \frac{u^{(i+1)} - u^{(i)}}{\delta t}, \\ -\frac{1}{\epsilon}\frac{\delta E}{\delta u} &\to A[u^{(i+1)}] + B[u^{(i)}]\end{aligned}$$

where the terms that are linear in u are rendered as part of the implicit operator $A[u^{(i+1)}]$ and the term that are non-linear in u are rendered as part of explicit

operator $B[u^{(i)}]$. The result is

$$\begin{aligned}
\frac{u^{(i+1)} - u^{(i)}}{\delta t} &= A[u^{(i+1)}] + B[u^{(i)}], \\
A[u^{(i+1)}] &= \left[\gamma \Delta u^{(i+1)} - \tilde{\kappa} \Delta^2 u^{(i+1)}\right], \\
B[u^{(i)}] &= \left[\tilde{\kappa}\left(\frac{1}{\epsilon^2}\Delta W'(u^{(i)}) - \frac{1}{\epsilon^4} W'(u^{(i)}) W''(u^{(i)}) + \frac{1}{\epsilon^2}\Delta u^{(i)} W''(u^{(i)})\right)\right. \\
&\qquad \left. -\frac{\gamma}{\epsilon^2} W'(u^{(i)}) - \frac{2M(\epsilon)}{\epsilon}\left(\int_\Omega u^{(i)}\, dx - A\right)\right].
\end{aligned}$$

Rearranging terms we get:

$$\begin{aligned}
u^{(i+1)} &- (\delta t \cdot \gamma)\Delta u^{(i+1)} + (\delta t \cdot \tilde{\kappa})\Delta^2 u^{(i+1)} = \\
&u^{(i)} + \delta t \left[\tilde{\kappa}\left(\frac{1}{\epsilon^2}\Delta W'(u^{(i)}) - \frac{1}{\epsilon^4} W'(u^{(i)}) W''(u^{(i)})\right.\right. \\
&\left.\left. + \frac{1}{\epsilon^2}\Delta u^{(i)} W''(u^{(i)})\right) - \frac{\gamma}{\epsilon^2} W'(u^{(i)}) - \frac{2M(\epsilon)}{\epsilon}\left(\int_\Omega u^{(i)}\, dx - A\right)\right].
\end{aligned}$$

Using the above equation, our program runs according to this algorithm:

1. Given an initial configuration $u^{(i)}$, calculate the right hand side.
2. Solve for $u^{(i+1)}$ using the Fourier Spectral Method.
3. Measure energy of $u^{(i+1)}$.
4. Start process over using $u^{(i+1)}$.
5. Stop when energy has leveled out.

In our experiments, the domain size is 6 by 6 grid with a 128 x 128 mesh, $\epsilon = 0.4$, $\tilde{\kappa} = \gamma = 1$, $M(\epsilon) = 1$, and $\delta t = 1 \times 10^{-5}$. We run simulations for several types of initial configurations: circle, ellipse, and "bean" shape. The results are quite uniform: u converges to characteristic function of a circle with interior area A. This confirms the expected: given a fixed enclosed area the bending energy and surface energy are minimized when the containing curve is a circle.

The Seifert Functional

Next we look at a functional that involves both an area constraint and a perimeter constraint.

$$\mathcal{E}_s[u] = \int_\Omega \frac{1}{\epsilon}\left[-\epsilon\Delta u + \frac{W'(u)}{\epsilon}\right]^2 dx + M_1\left(\frac{\epsilon}{2}|\nabla u|^2 + \frac{1}{\epsilon}W(u) - P\right)^2 + M_2\left(\int_\Omega u - A\right)^2.$$

We name this functional, $\mathcal{E}_s(u)$, the "Seifert Phase Field Functional" in reference to Seifert's classic work on the equivalent sharp interface problem [35]. The steepest descent problem corresponding to this new functional is

$$\begin{aligned}\frac{\partial u}{\partial t} = -\frac{1}{\epsilon}\frac{\delta L}{\delta u} = &-\frac{\tilde{\kappa}}{\epsilon}\left[\epsilon\Delta^2 u - \frac{1}{\epsilon}\Delta W'(u) + \frac{1}{\epsilon^3}W'(u)W''(u) - \frac{1}{\epsilon}\Delta u W''(u)\right] \\ &- \frac{2M_1}{\epsilon}\left(\frac{\epsilon}{2}|\nabla u|^2 + \frac{1}{\epsilon}W(u) - A\right)\left(-\epsilon\Delta u + \frac{1}{\epsilon}W'(u)\right) \\ &- \frac{2M_2}{\epsilon}\left(\int_\Omega u\, dx - V\right).\end{aligned}$$

This equation can be solved using the Semi-Implicit scheme

$$\begin{aligned}&u^{(i+1)} + (\delta t\cdot\tilde{\kappa})\Delta^2 u^{(i+1)} = \\ &\quad u^{(i)} + \delta t\left[\tilde{\kappa}\left(\frac{1}{\epsilon^2}\Delta W'(u^{(i)}) - \frac{1}{\epsilon^4}W'(u^{(i)})W''(u^{(i)}) + \frac{1}{\epsilon^2}\Delta u^{(i)}W''(u^{(i)})\right)\right. \\ &\quad - \frac{2M_1(i)}{\epsilon}\left(\frac{\epsilon}{2}|\nabla u^{(i)}|^2 + \frac{1}{\epsilon}W(u^{(i)}) - P\right)\left(-\epsilon\Delta u^{(i)} + \frac{1}{\epsilon}W'(u^{(i)})\right) \\ &\quad \left. -\frac{2M_2(i)}{\epsilon}\left(\int_\Omega u^{(i)}\, dx - A\right)\right].\end{aligned}$$

To enforce the constraints in these simulations, we increase the penatly coefficients as the simulation progresses: $M_1(i) = M_2(i) = 0.1\cdot i$. The other parameters are the same as before.

4.2.2 Results

We run simulations for four types of starting configurations and various area/perimeter constants, A and P. We observe a diverse family of minimal configurations which depend on the initial configuration and increase in complexity

as P/A increases. In Figures 4.4–4.6, we show the recovery of some vesicle shapes also present in nature. In each row of these figures, the first picture is the initial configuration, the last picture is the steady state solution, and the two picture in between are intermediate states of u. In the red region u is 1 and in the blue region u is 0. The transition region in between the blue and red regions has width approximately $\epsilon = 0.4$.

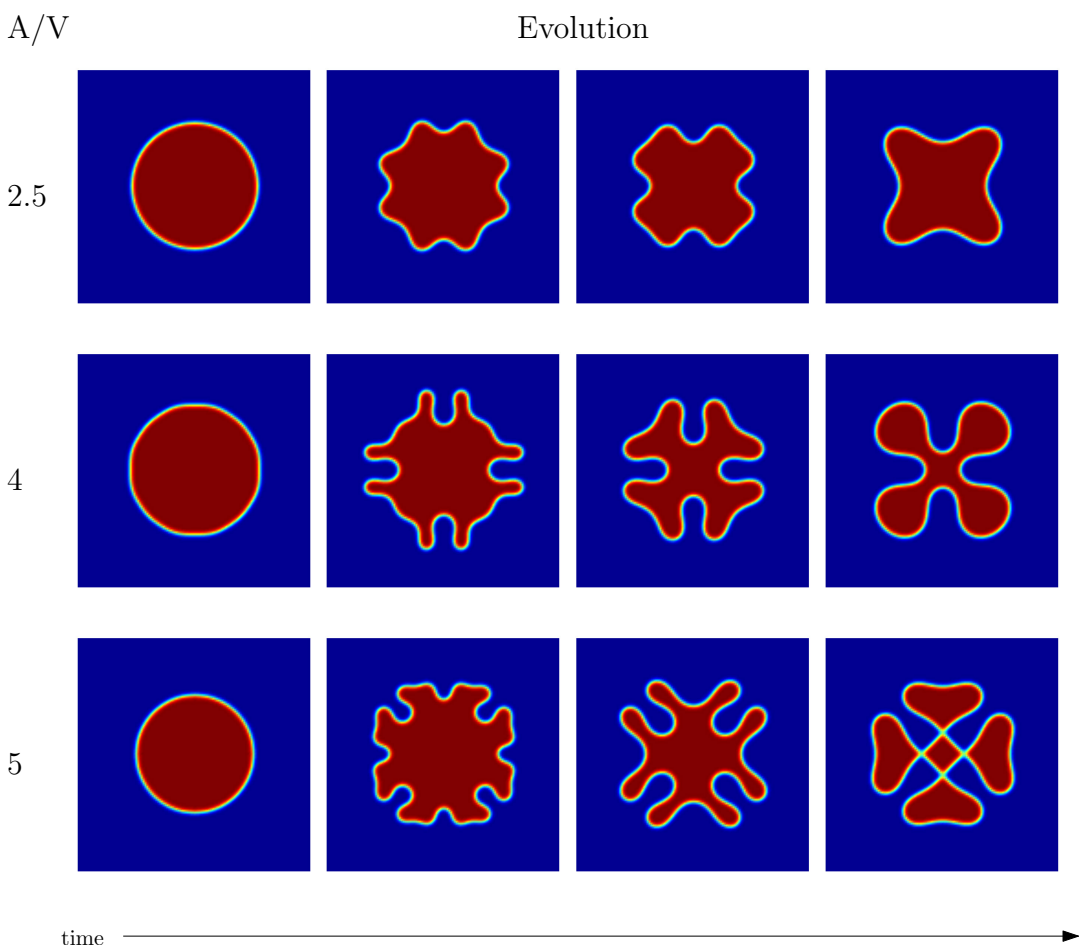

Figure 4.4: Configurations started with a circle.

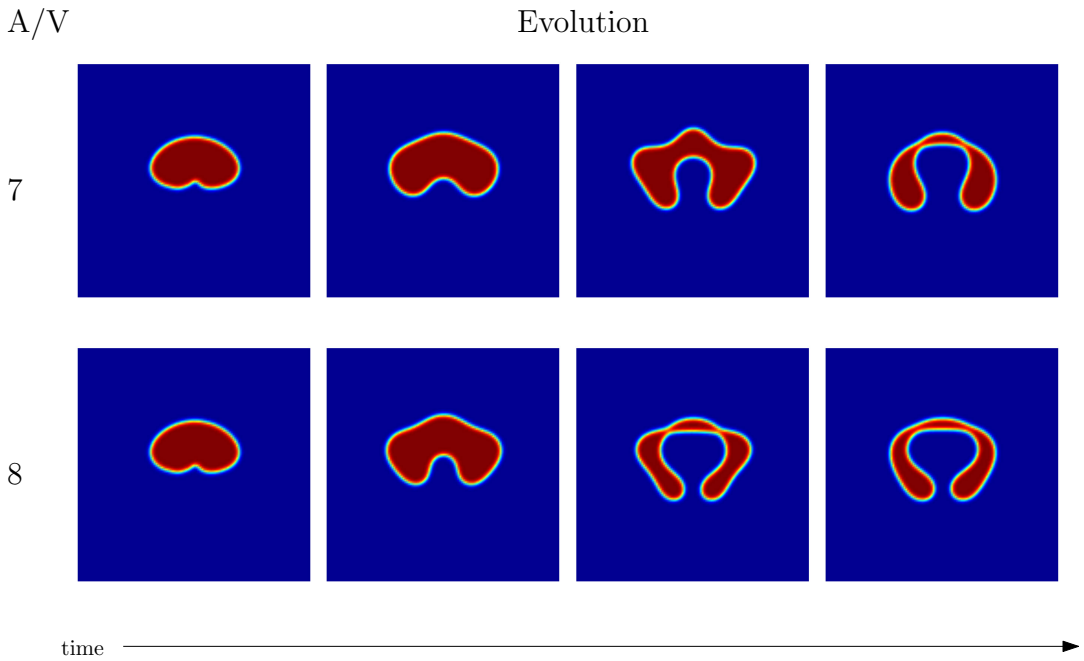

Figure 4.5: Configurations started with a "bean".

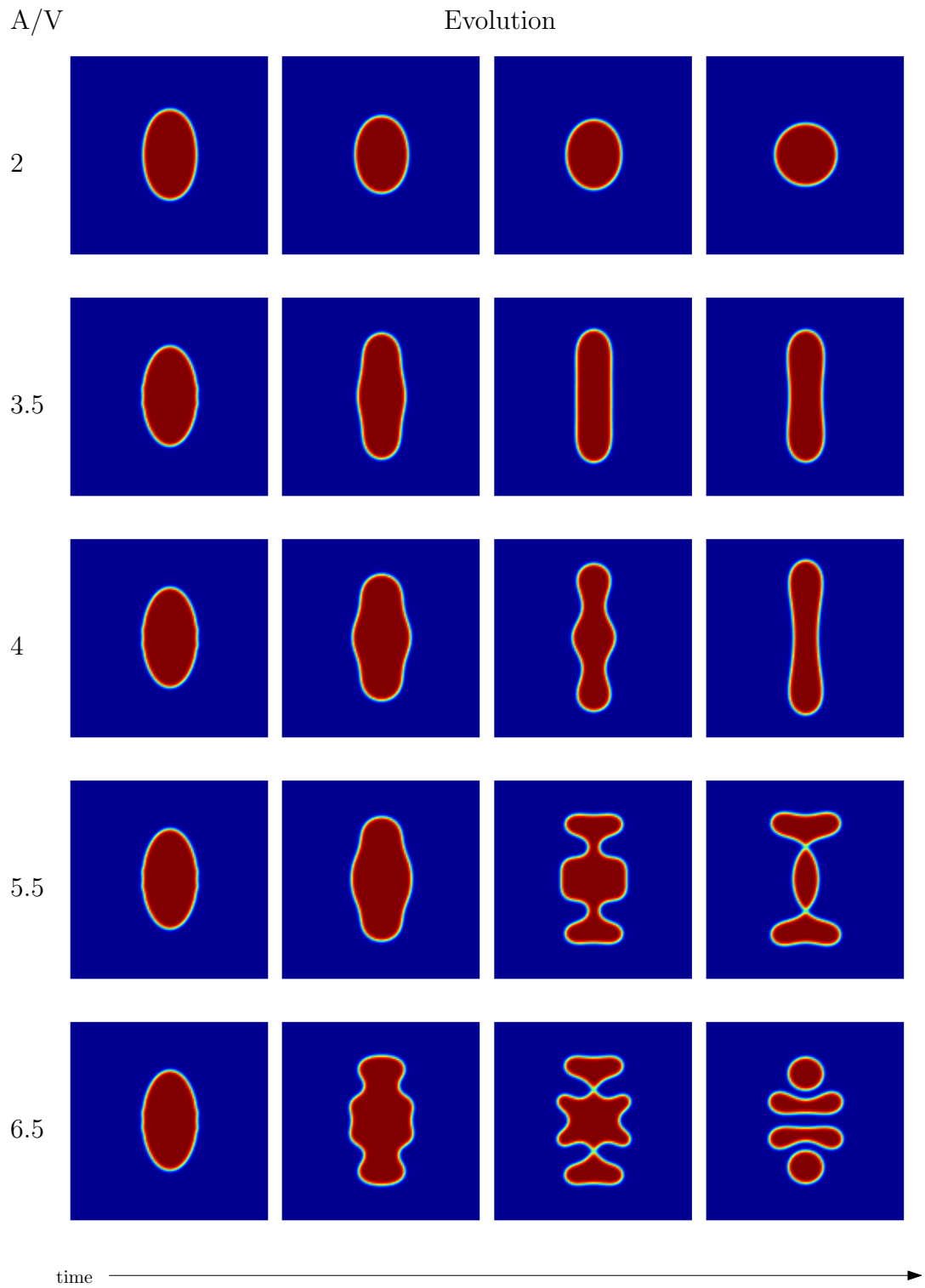

Figure 4.6: Configurations started with an ellipse.

4.3 3D Simulations: Shapes and Betti Numbers

4.3.1 Setup

In this section, we implement a Semi-Implicit Fourier Spectral Method to find the minimizers of the 3D version of the aforementioned Seifert Phase Field Functional with a bending energy and area and volume constraint penalty terms:

$$\mathcal{E}[u] = \int_\Omega \frac{1}{\epsilon}\left[-\epsilon\Delta u + \frac{W'(u)}{\epsilon}\right]^2 dx + M_1\left(\frac{\epsilon}{2}|\nabla u|^2 + \frac{1}{\epsilon}W(u) - A\right)^2 + M_2\left(\int_\Omega u - V\right)^2.$$

We solve the steepest descent problem corresponding to this functional using a Semi-Implicit scheme which gives us the following ordinary differential equation:

$$\begin{aligned} &u_{i+1} + (\delta t \cdot \tilde{\kappa})\Delta^2 u_{i+1} = \\ &\quad u_i + \delta t\left[\tilde{\kappa}\left(\frac{1}{\epsilon^2}\Delta W'(u_i) - \frac{1}{\epsilon^4}W'(u_i)W''(u_i) + \frac{1}{\epsilon^2}\Delta u_i W''(u_i)\right)\right. \\ &\quad - \frac{2M_1(i)}{\epsilon}\left(\frac{\epsilon}{2}|\nabla u_i|^2 + \frac{1}{\epsilon}W(u_i) - A\right)\left(-\epsilon\Delta u_i + \frac{1}{\epsilon}W'(u_i)\right) \\ &\quad \left. -\frac{2M_2(i)}{\epsilon}\left(\int_\Omega u_i\, dx - V\right)\right]. \end{aligned}$$

As in the previous experiments, we start with an initial profile $u^{(0)}$. At each time step we apply the Fourier Spectral method to solve this ordinary differential equation for $u^{(i+1)}$. This process is iterated until the energy stabilizes, then, we take $u^{(i)}$ as our solution.

In these experiments, the domain size is 6 by 6 by 6 region with a 64 x 64 x 64 mesh, $\epsilon = .4$, $\tilde{\kappa} = 1$, $M_2(i) = M_1(i) = 0.1 \cdot i$, and $\delta t = 1 \times 10^{-4}$. We repeat the experiment for several initial profiles: sphere, ellipsoid, blood cell shape, and parachute shape.

4.3.2 Results

We once again observe a diverse range of minimal configurations. The final configuration depends on the choice of initial profile. The evolution of the phase field over time tends to obey the patterns of evolution described in Figures 4.7 and 4.8. For a low area-to-volume ratio the phase field usually stops evolving at phase 2 or 3. For higher area-to-volume ratios the phase field progresses to phase 5 or 6.

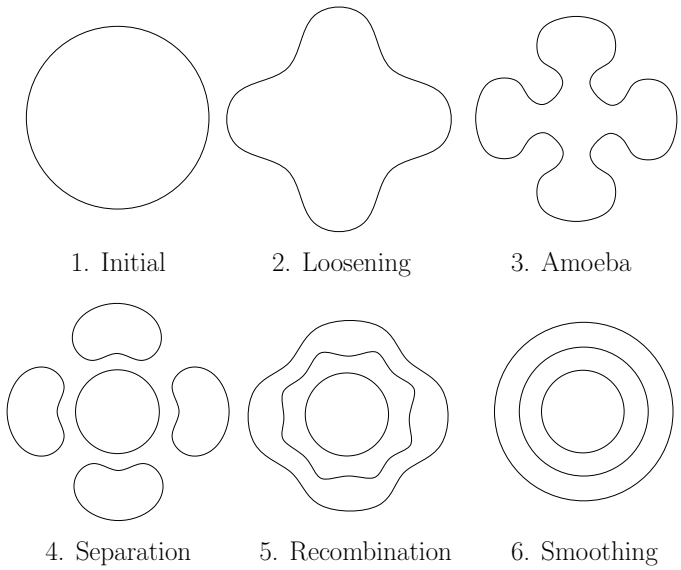

Figure 4.7: Evolution of the 3D phase field. Initial profile is a sphere.

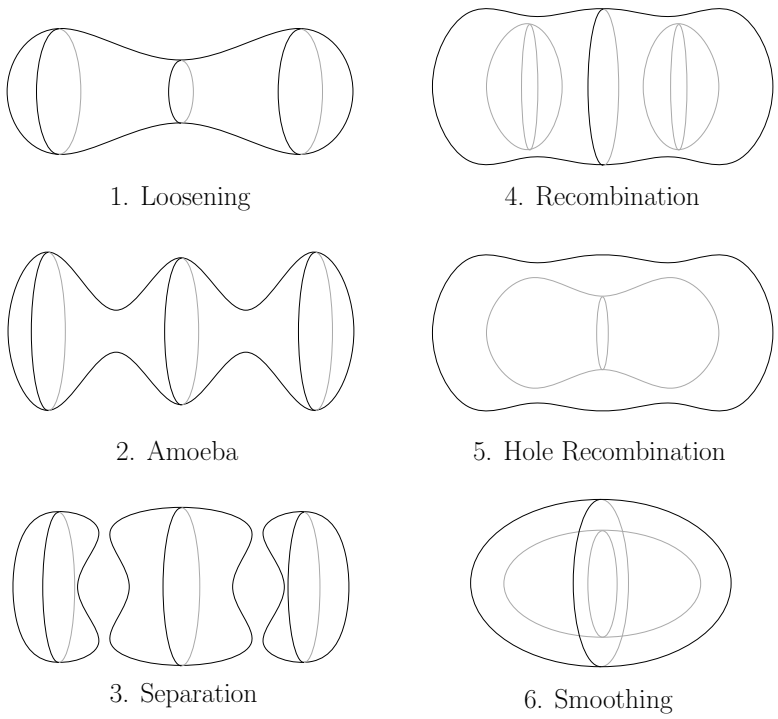

Figure 4.8: Evolution of the 3D phase field. Initial profile is an ellipsoid. Grey lines show the boundary of the interior regions and the shape of the back side of the configuration.

To visualize how the program is finding the minimizer, we plot in Figures 4.9 through 4.11 the 1/2 level sets of the initial function $u^{(0)}$, the steady state function $u^{(\infty)}$, and two intermediate configurations. The configurations are subdivided by initial states and ordered by increasing area-to-volume ratio.

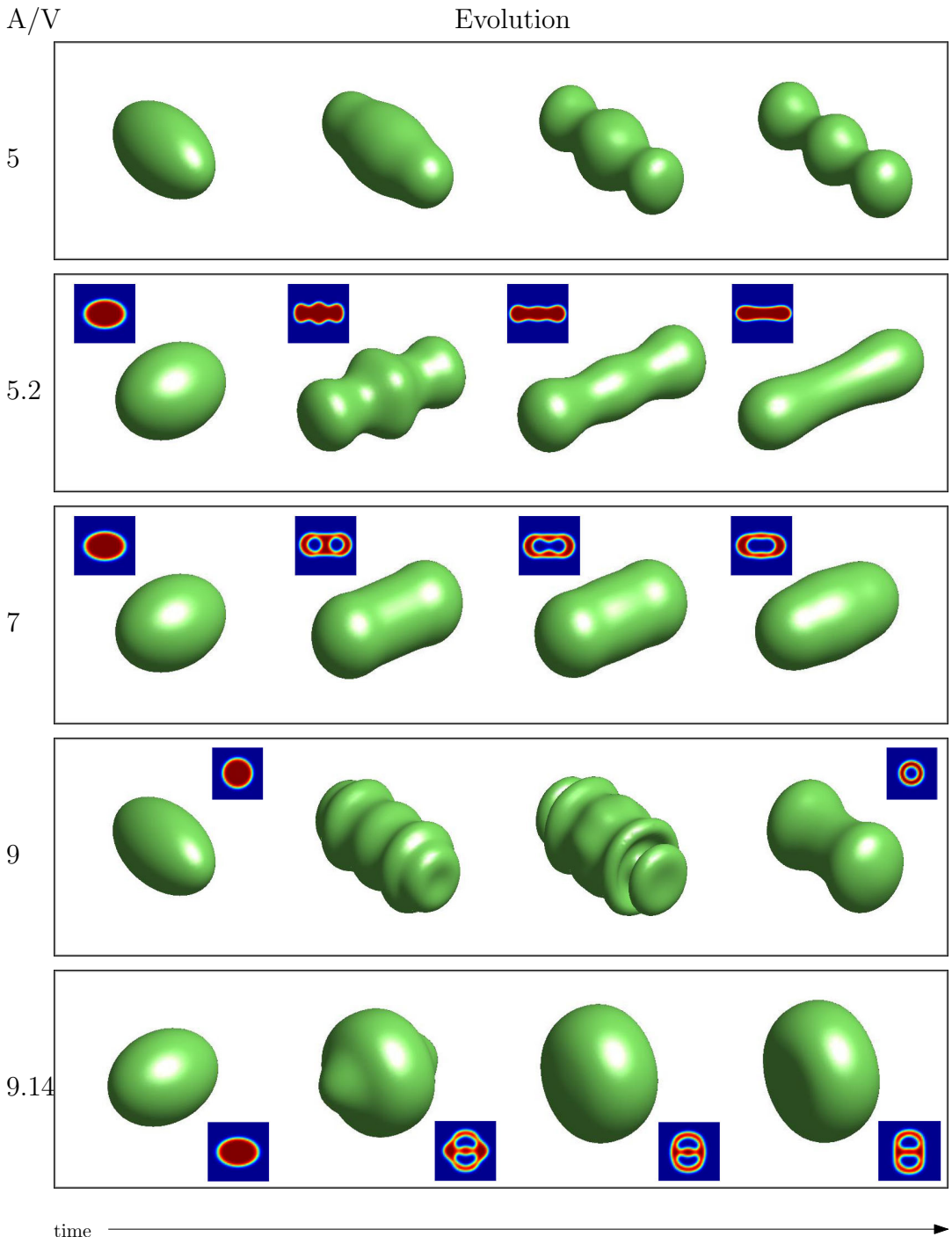

Figure 4.9: Configurations started with an ellipsoid.

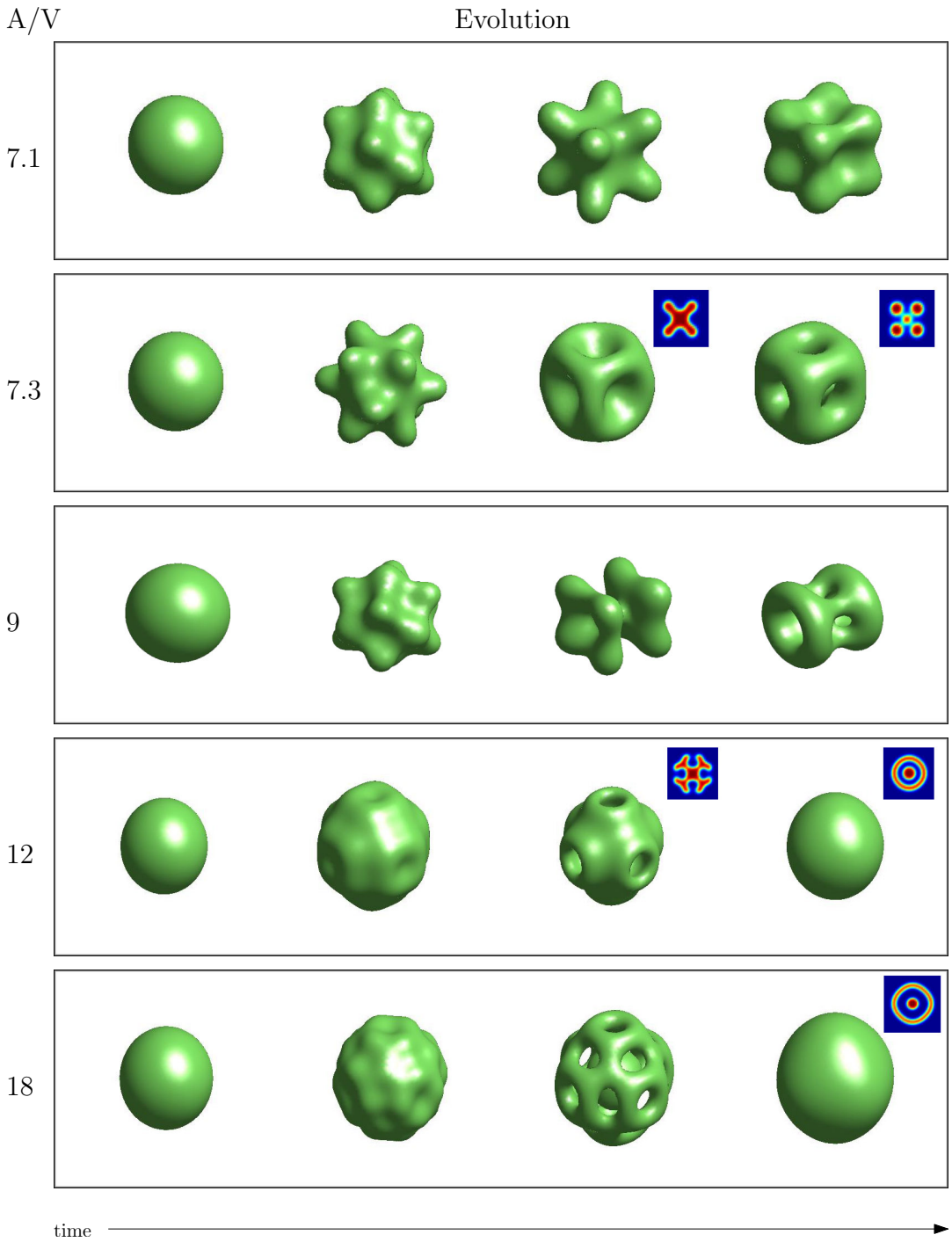

Figure 4.10: Configurations started with a sphere.

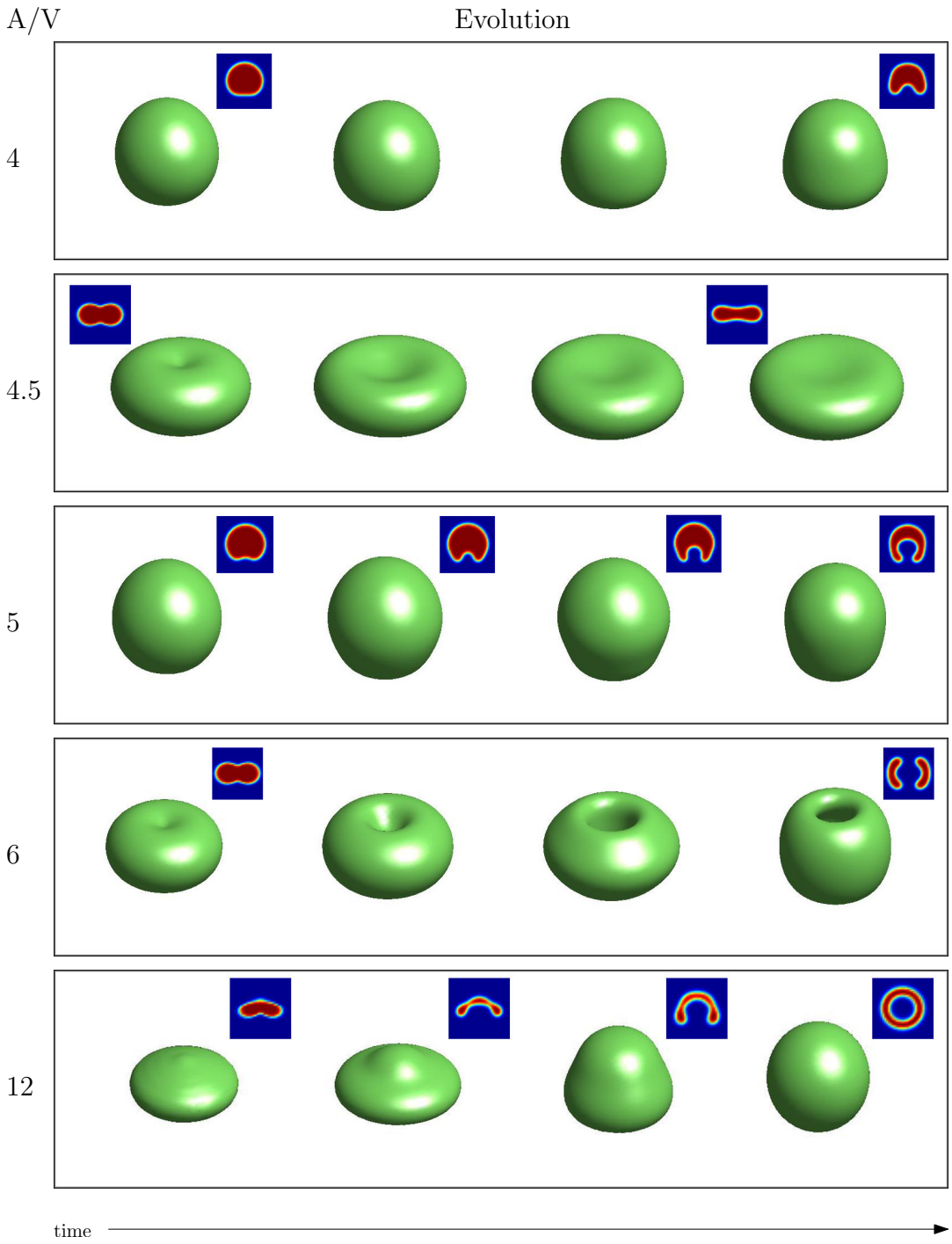

Figure 4.11: Configurations started with a blood cell, dented bubble, or a parachute shape.

In the Figures 4.12 and 4.13 we see how the energy varies with time and area-to-volume ratio. The plots in Figure 4.12 demonstrate that the program is finding a lower energy configuration. The initial increase in the bending energy is due to the configurations desire to satisfy the area and volume constraints.

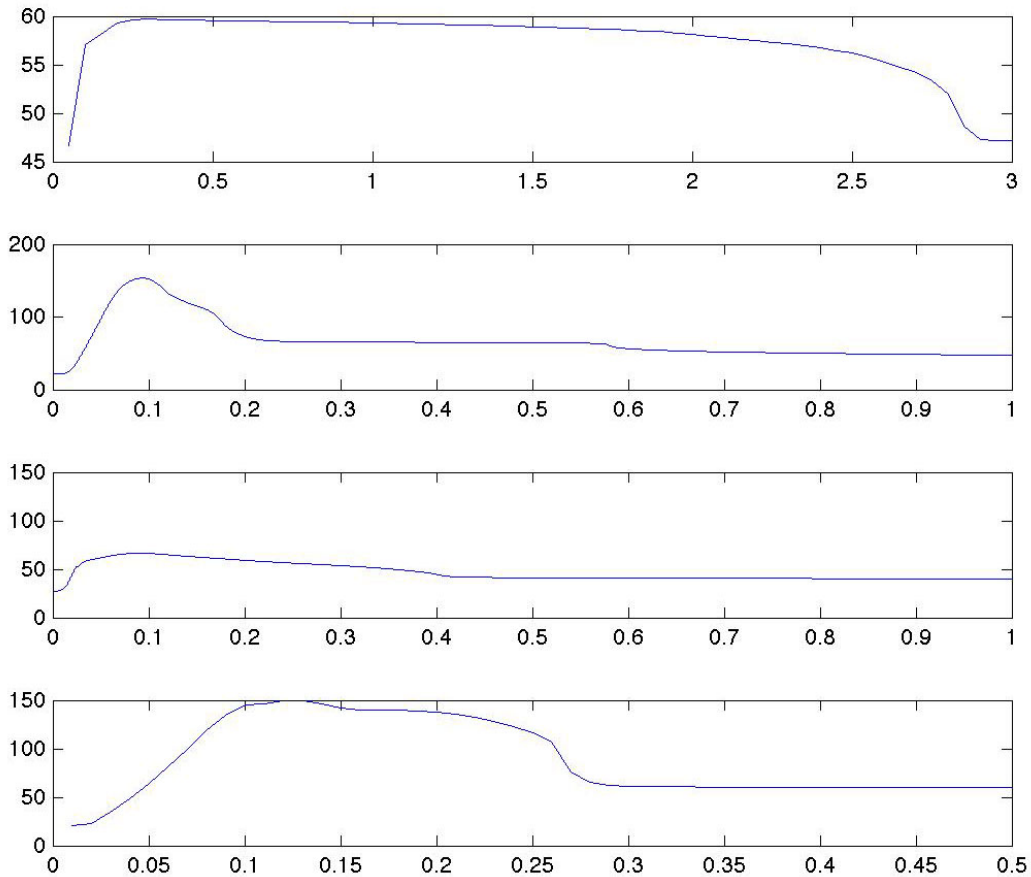

Figure 4.12: Energy versus time plots for selected starting configurations and area-to-volume ratios. From top to bottom: parachute with A/V of 12, ellipsoid with A/V of 7, blood cell with A/V of 6, and sphere with A/V of 8.

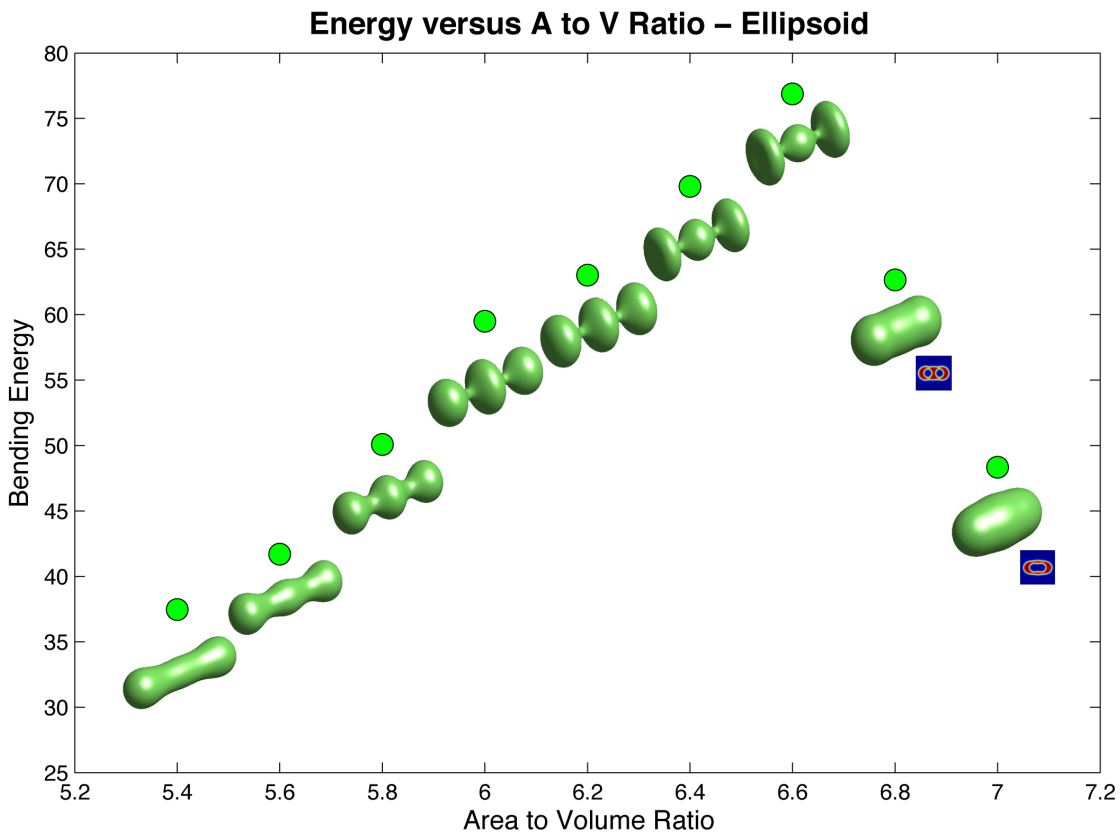

Figure 4.13: Energy versus Area-to-Volume ratio plot for simulations that start with an ellipsoid.

4.3.3 Classification of Configurations with Betti Numbers

In our simulations, we observe a wide variety of new 3D configurations. As a way of classifying these shapes, we compute their Betti numbers. Betti numbers are commonly used to classify complex 3D configurations in various modeling contexts including data analysis [8] and polycrystalline materials study [38].

Formally, the kth Betti number of X is the rank of the kth homology group, $H_k(X)$. For simple closed surfaces the first three Betti numbers have a nice intuitive interpretation: the first Betti number counts the number of connected components, the second Betti number counts the number of one dimensional holes, and the third Betti number counts the number of two dimensional holes or enclosed regions.

Steady-State Profile	B_0	B_1	B_2	Steady-State Profile	B_0	B_1	B_2
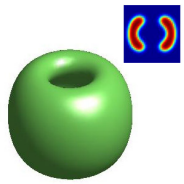 BC, VA 6	1	2	1	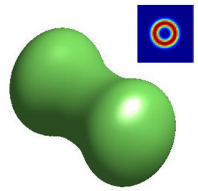 E3, VA 9	2	0	2
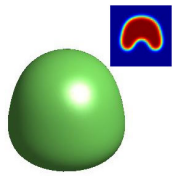 P, VA 4	1	0	1	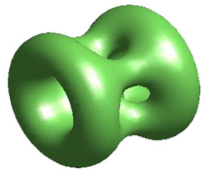 S, VA 9	1	7	21
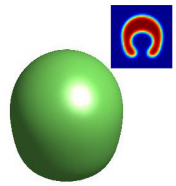 P, VA 5	1	0	1	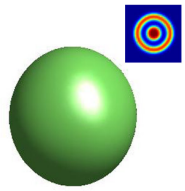 S, VA 12	3	0	3
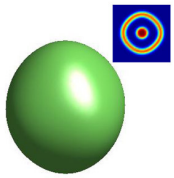 S, VA 18	3	0	3	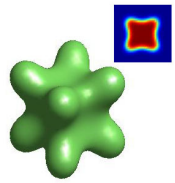 S, VA 7.1	1	0	1

Figure 4.14: Table 1 of Betti numbers for minimizers.

VA = Volume-to-area ratio,

P = Initial configuration was dented bubble (see first diagram in figure 4.11),

S = Initial configuration was sphere,

E2 (3) = Initial configuration was ellipsoid with length 2 (3) times it width,

BC = Initial configuration was blood cell (see fourth diagram in figure 4.11).

Steady-State Profile	B_0	B_1	B_2	Steady-State Profile	B_0	B_1	B_2
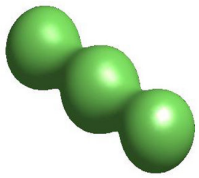 E3, VA 5	1	0	1	 E3, VA 7	1	0	1
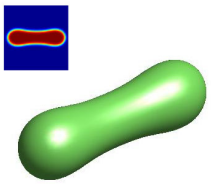 E2, VA 5.2	1	0	1	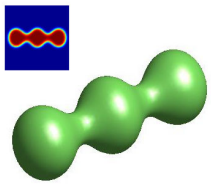 E2, VA 5.8	1	0	1
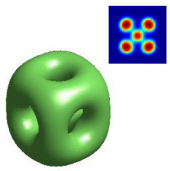 S, VA 8	2	7	22	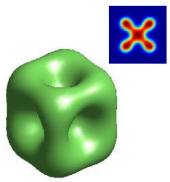 S, VA 7.2	1	0	1
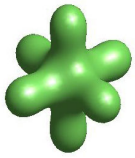 S, VA 7.18	1	0	1	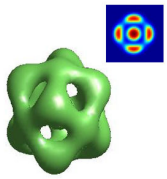 S, VA 9, H 2	2	10	46

Figure 4.15: Table 2 of Betti numbers for minimizers.

Chapter 5

Conclusions and Future Directions

5.1 Summary

This dissertation has four main results:

1. We have shown that minimizers of
$$E_\epsilon[u] = \int_\Omega \left[\frac{\epsilon}{2}|\nabla u|^2 + \frac{1}{\epsilon}W(u)\right] dx + M(\epsilon)\left(\int_\Omega u\,dx - V\right)^2$$
converge to minimizers of the sharp interface problem
$$\int_\Gamma dS \quad \text{with (volume enclosed by } \Gamma) = \mathrm{V}_0$$
by proving Gamma-convergence of the former functional to the latter.

2. We have shown that minimizers of
$$\mathcal{E}_\epsilon[u] = \int_\Omega \left[\frac{\epsilon}{2}|\nabla u|^2 + \frac{1}{\epsilon}W(u)\right] dx + M(\epsilon)\left(\int_\Omega u\,dx - V\right)^2 + \int_\Omega \frac{1}{\epsilon}\left[-\epsilon\Delta u + \frac{W'(u)}{\epsilon}\right]^2 dx$$
converge to minimizers of the sharp interface problem
$$\int_\Gamma H^2 dS + \int_\Gamma dS \quad \text{with volume enclosed by } \Gamma = \mathrm{V}_0$$
by proving Gamma-convergence of the former functional to the latter.

3. We have created a program that uses a Semi-Implicit Fourier Spectral method to search for the minimizers of the Shao–Rappel–Levine phase field functional. We have also written a similar program that searches for minimizers of the closely related Seifert Phase Field Functional with non-zero spontaneous curvature. This gives us a good way of solving Seifert's classic problem:

$$\begin{gathered}\text{Find } \Gamma \text{ that minimizes } \textstyle\int_\Gamma (H-H_0)^2 dS \\ \text{subject to} \\ (1) \text{ Volume enclosed by } \Gamma = V_0 \\ \text{and } (2) \text{ Surface area of } \Gamma = A_0\end{gathered}$$

4. Using these programs we have found several phase field configurations whose level sets are known minimizers of the sharp interface problem. We have also observed a "zoo" of interesting minimizing configurations and classified these steady state minimizers with Betti numbers.

5.2 Future Problems

There are several interesting directions of further research.

1. In the spirit of Seifert [35] one could explore the space of 3D configurations of vesicles given various volume and area constraints and spontaneous curvatures. The sharp interface model's dependence on H_0, V, and A is partially known in radially symmetric case, but the asymmetric configurations are almost completely unexplored.

2. In the literature [13], the bending energy with spontaneous curvature has been modeled with the phase field functional

$$B_\epsilon[u] = \int_\Omega \frac{1}{\epsilon}\left[-\epsilon\Delta u + \frac{W'(u)}{\epsilon} + H_0\left|u(1-u)\right|\right]^2 dx. \tag{5.1}$$

Alternatively one could explore a bending energy with spontaneous curvature implemented like so:

$$\tilde{B}_\epsilon[u] = \int_\Omega \frac{1}{\epsilon}\left[-\epsilon\Delta u + \frac{W'(u)}{\epsilon} + \epsilon H_0|\nabla u|\right]^2 dx. \tag{5.2}$$

The following lemma motivates this modification:

Lemma 5.2.1. *Let* $u_\epsilon = \frac{1}{2}\left[1 - \gamma\left(\frac{h(x)}{\epsilon}\right)\right]$ *where* $\gamma = tanh(t)$ *and* $h(x)$ *is distance from some* χ_A *where* A *is open and* ∂A *is* C^2*. Then, for* $\tilde{B}_\epsilon[u_\epsilon]$ *as defined in 5.2,*

$$\lim_{\epsilon\to 0} \tilde{B}_\epsilon[u_\epsilon] = \int_{\partial A} (\boldsymbol{H}_{\partial A} - H_0)^2 d\mathcal{H}_{n-1}.$$

3. Since our configurations sometimes go through topological changes, one might consider reintroducing the Gaussian curvature part of the bending energy. This proves difficult to impliment in simulations, mostly due to the "quanta" nature of such of a Gaussian energy. However, a rudimentory method for implementing Gaussian curvature into a phase field model have been suggested by Du et al [12].

4. One could also employ different numerical methods to solve the fourth-order steepest descent problem. The advantage of the fourier spectral method is speed; simulations run on the order of 10-20 minutes which for a fourth-order non-linear equation is excellent. However, for small episilon (less than 3% of the domain width) the minimizer's jump discontinuity at the interface invokes the Gibbs phenomenon and makes the program unstable. The instability can be fixed by further discretization of the domain and smaller time steps, but simulation run time is greatly increased.

5. On the analysis side of things, one could generalize the Gamma-convergence results from Chapter 3 and prove Gamma-convergence in the case of non-smooth limit functions. Because the boundary curvature of sets with a boundary that is not smooth is not well-defined, one would have to use a generalized form of curvature. Masnou and Nardi [24] have suggested that the tools of Geometric Measure Theory, in particular Young's measures and varifolds [27], would be aptly suited for such a task.

6. One could also generalize our Gamma-convergence results for a bending energy that includes spontanous curvature. For smooth limit functions the right limsup inequality is easily established (see Lemma 5.2.1). However, the

liminf inequality would be much harder and would likely involve Geometric Measure Theory methods similar to those of Roger and Schätzle [28].

7. Finally, one could look at the sharp interface limit of the phase field equations with the Actin-Myosin term and coupled PDEs [34].

Bibliography

[1] Anderson, D.M.; McFadden, G.B.; Wheeler, A.A. (1998) A diffuse-interface methods in fluid mechanics. *Ann. Rev. Fluid Mech.* 30, 139–165.

[2] Bellettini, G.; Mugnai, L. (2010) Approximation of the Helfrich's functional via diffuse interfaces. *SIAM J. Math. Anal.* Vol. 42, No. 6, pp. 2402–2433.

[3] Bellettini, G.; Paolini, M. (1993) Approximazione variazionale di funzionali con curvatura. *Seminario di Analisi Matematica, Dipartimento do Matematica dell'Universita di Bologna. Technoprint Bologna,* pp. 87–97.

[4] Braides, A. (2002) Gamma-Convergence for Beginners. *Oxford University Press.*

[5] Biben, T.; Misbah, C. (2003) Tumbling of vesicles under shear flow within an advected-field approach. *Phys. Rev. E* 67, p. 031908.

[6] Cahn, J.; Hilliard, J. (1958) Free energy of a nonuniform system. I. interfacial free energy. *The Journal of Chemical Physics*, 28, pp. 258–268.

[7] Canham, P.B. (1970) The minimum energy of bending as a possible explanation of the biconcave shape of the red blood cell. *J. Theor. Biol.*, 26, pp. 61–81.

[8] Carlsson, G. (2009) Topology and Data. *Bulletin of AMS*, Volume 46, No. 2, pp. 255–308.

[9] Dal Maso, G. (1993) An introduction to Gamma-convergence. *Birkhuser, Basel.*

[10] Deseri, L.; Piccioni, M. D.; Zurlo, G. (2008) Derivation of a new free energy for biological membranes *Conti. Mech.* & *Thermodyn.* Oct 2008, Vol. 20 Issue 5, p255.

[11] Deserno, M. Fluid lipid membranes: a primer.

[12] Du, Q.; Liu, C.; Wang, X. (2005) Retrieving topological information for phase field models. *SIAM J. Appl. Math.* Vol. 65, No. 6, pp. 1913–1932.

[13] Du, Q.; Liu, C.; Ryham, R.; Wang, X. (2005) Modeling the spontaneous curvature effects in static cell membrane deformations by a phase field formulation. *Comm. on Pure and Appl. Analysis.* Vol. 4, No. 4, pp. 537–548.

[14] Evans, L. C. (2010) Partial Differential Equations, 2nd edition. *American Math Society.*

[15] Evans, L. C. (1992) Measure Theory and Fine Properties of Functions. *CRC Press.*

[16] Fleming, W. H.; Rishel, R. W. (1960) An integral formula for total gradient variation. *Arch. Math.,* 11, pp. 218–222

[17] Helfrich, W. (1973) Elastic properties of lipid bilayers: theory and possible experiments. *Z. Naturforsch.* 28c, pp. 692–703.

[18] Israelachvili, J. (2002) Intermolecular and Surface Forces. 2nd edition. *Academic Press.*

[19] Karma, A.; Kessler, D. A.; Levine, H. (2001) Phase-Field Model of Mode III Dynamic Fracture *Phys. Rev. Lett.* 87, p. 045501.

[20] Keller, P; Sternberg, P.; Rubinstein, J. (1989) Fast reaction, slow diffusion and curve shortening. *SIAM J. Appl. Math.* 49. pp. 116–133.

[21] Keren, K; Pincus, K; Allen, G. M.; Barnhart E. L.; Marriott, G.; Mogilner, A.; and Theriot, J. A. (2008) Mechanism of shape determination in motile cells. *Nature (London)* 453, pp. 475–480.

[22] Korlach, J.; Schwille P.; Webb, W. W.; Feigenson, G. W. (1999) Characterization of lipid bilayer phases by confocal microscopy and fluorescence correlation spectroscopy. *Proc. Natl. Acad. Sci.* USA, Vol. 96, pp. 8461–8466.

[23] Liu, C; Ryham, R; Wang, X; and Du, Q (2005) A phase field formulation of the Willmore problem. *Nonlinearity* 18; 1249–1267.

[24] Masnou, S.; Nardi, G. (2012) Gradient Young measures, varifolds, and a generalized Willmore functional. *arXiv* 10.1515/acv-2011-0014.

[25] McFadden, G.B.; Wheeler, A.A.; Anderson, D.M. (2000) Thin interface asymptotics for an energy/entropy approach to phase-field models with unequal conductivities. *Physica D: Nonlinear Phenomena*, Volume 144. pp. 154–168.

[26] Modica, L. (1987) The gradient theory of phase transitions and the minimal interface criterion. *Arch. Rational Mech. Anal.* 98(2), pp. 123–142.

[27] Morgan, F. (2009) Geometric Measure Theory: A Beginner's Guide. 4th edition. *Academic Press Inc.*

[28] Roger, M.; Schätzle, R. (2006) On a modified conjecture of De Giorgi. *Math Z* 254, pp. 675–714.

[29] Sackmann, E. (1994) Membrane bending energy concept of vesicle and cell-shapes and shape-transitions. *FEBS Lett.* 436, pp. 3–16

[30] Safran, S. A. (1999) Curvature elasticity of thin films. *Advances in Physics*, 48:4, pp. 395–448.

[31] Safran, S. A. (2003) Statistical Thermodynamics of Surfaces, Interfaces, Membranes. *Westview Press.*

[32] Schätzle, R. (2009) Lower semicontinuity of the Willmore functional for currents. *J. Differential Geom.* Volume 81, Number 2, pp. 437–456

[33] Shao, D.; Rappel, J.; Levine, H. (2010) Computational model for cell morphodynamics. *Phys. Rev. Lett.* 105, pp. 108–104.

[34] Shao, D. (2011) Computational model for cell migration. *Dissertation*, UCSD, Biophysics.

[35] Seifert, U. (1997) Configurations of fluid membranes and vesicles. *Advances in Physics*, Vol 46, No 1, pp. 13–137.

[36] van der Waals, J. D. (1893) The thermodynamic theory of capillarity under the hypothesis of a continuous density variation. *J. Stat. Phys.*, 20, pp. 197–244, (English version 1979).

[37] Wang, Z; Wang, J; Li, J; Yang, G; Zhou, Y (2011) Quantitative investigation of cellular growth in directional solidification by phase-field simulation. *Phys. Rev. E.* 84, p. 041604.

[38] Wanner, T.; Fuller, E., Saylor, D. (2010) Homology metrics for microstructure response fields in polycrystals. *Acta Materialia* 58, pp. 102–110.